



## Dry deposition effect of urban green spaces on ambient particulate matter pollution in China

Jiaqi Yao<sup>a</sup>, Shuqi Wu<sup>b</sup>, Yongqiang Cao<sup>a,\*</sup>, Jing Wei<sup>c</sup>, Xinming Tang<sup>d</sup>, Liuru Hu<sup>e</sup>, Jianjun Wu<sup>a</sup>, Huicai Yang<sup>a</sup>, Jianhua Yang<sup>a</sup>, Xinhui Ji<sup>a</sup>

<sup>a</sup> Academy of Eco-civilization Development for JING-JIN-JI Megalopolis, Tianjin Normal University, Tianjin 300387, China

<sup>b</sup> School of Resource, Environment and Tourism, Capital Normal University, Beijing 100048, China

<sup>c</sup> Department of Atmospheric and Oceanic Science, Earth System Science Interdisciplinary Center, University of Maryland, College Park, MD, USA

<sup>d</sup> Land Satellite Remote Sensing Application Center (LASAC), Ministry of Natural Resources of P.R. China, Beijing 100048, China

<sup>e</sup> Dpto. de Ingeniería Civil, Escuela Politécnica Superior de Alicante, Universidad de Alicante, P.O. Box 99, E-03080 Alicante, Spain



### ARTICLE INFO

Editor: Jianmin Chen

**Keywords:**

Dry deposition effect  
Satellite remote sensing  
UFORE

Wavelet coherence  
Spatiotemporal analysis

### ABSTRACT

Particulate matter (PM) is a major source of urban air pollution that poses a serious threat to the environment and human health. This study quantified the dry deposition effect of PM<sub>2.5</sub> and PM<sub>10</sub> on vegetation using a mathematical model to overcome the limitations of traditional site-scale research. Additionally, multi-source satellite remote sensing products were combined to form a raster dataset to estimate the effect of dry deposition on PM<sub>2.5</sub> and PM<sub>10</sub> in China's urban green spaces from 2000 to 2020. The spatial and temporal changes in the long-term series were analyzed, and the influence of environmental factors on dry deposition was analyzed in combination with wavelet changes. The experimental results showed that: 1) from 2000 to 2020, the dry deposition effect of PM<sub>2.5</sub> and PM<sub>10</sub> on vegetation showed an initial increasing and then decreasing trend caused by the sudden drop in atmospheric pollutant particle concentration driven by local policies; 2) broad-leaved forests provided the main dry deposition effects in urban spaces, accounting for 89.22 %, indicating a need to increase the density of these forest types in urban development planning to improve air quality; and 3) PM<sub>2.5</sub>, PM<sub>10</sub>, and environmental impact factors have time-frequency scale coherences, and the coherence between PM<sub>2.5</sub> reduction and these factors is more complex than that of PM<sub>10</sub>, with precipitation being the best variable to explain the change in PM<sub>2.5</sub> and PM<sub>10</sub>. These findings are important for the prevention and control of urban air pollution, regional planning of green spaces, and sustainable development of cities.

### 1. Introduction

Due to the rapid rise of regional industrialization, urbanization, and economic growth, air pollution has significantly increased, thereby impeding the sustainable development of urban ecosystems. The increase in air pollution poses a significant risk of respiratory and cardiovascular diseases, while also altering regional climate and meteorological phenomena. Therefore, it is imperative to implement measures to prevent and control air pollution (Schwartz et al., 1996; Tai et al., 2010; Wang et al., 2020; Rahman et al., 2022). Particulate Matter (PM) encompasses solid or liquid particles such as dust, soot, and chemicals that become suspended in the air. These particles enter the atmosphere through industrial emissions, automobile exhaust, and agricultural and residential activities (Viana et al., 2008; Dominici et al.,

2014). PM represents a crucial component of urban air pollution (Beckett et al., 1998; Yang et al., 2005; Shah et al., 2022). The development of cities has raised significant environmental concerns regarding the reduction of PM emissions. Urban green spaces, comprising both artificial and natural green vegetation coverage within urban areas, including forest parks, river wetlands, and street green belts, play a crucial role in purifying the air in urban environments (Wu et al., 2012; Xie et al., 2017; Zhai et al., 2022a, 2022b). Air purification is either achieved by the direct interception and absorption of PM by vegetation through retention, attachment, and adhesion, or by changing meteorological factors such as wind fields. The dust retention effect is influenced by the canopy structure, growth stage, and leaf roughness of plants within the green space (Zhao et al., 2013; Chen et al., 2014; Fan et al., 2015; Zhai et al., 2022c).

\* Corresponding author.

E-mail address: [caoyongqiang@tjnu.edu.cn](mailto:caoyongqiang@tjnu.edu.cn) (Y. Cao).

The process of vegetation directly reducing atmospheric PM is known as dry deposition. However, accurately estimating this process using simple empirical mathematical relationships poses challenges (Pretzsch et al., 2015; DeJarnett et al., 2016). Early models predominantly relied on simplistic estimations of dry deposition processes by primarily considering theories in aerodynamics and micrometeorology. These models neglected the impact of plant structural characteristics and species variations, while also insufficiently quantifying several parameters (Davidson et al., 1982; Slinn, 1982). As research on dry deposition progresses, more advanced models have been developed, notably the widely utilized ENVI-met and Urban Forest Effects (UFORE) models (Hirabayashi, 2011; Velásquez Ciro et al., 2021). The ENVI-met model is a three-dimensional hydrodynamic model that effectively simulates the interaction among the subsurface, vegetation, and atmosphere. It is commonly employed for simulating urban microenvironments and assessing the effects of green spaces (Bruse and Fleer, 1998). In a study conducted by Vos et al. (2013) using ENVI-met, the effect of roadside green belt structure on atmospheric quality was investigated. The study indicated a positive correlation with depression and a negative correlation with permeability, although the underlying mechanism concerning vegetation remained unclear. The UFORE model, developed by the Northeast Forest Research Centre of the United States Department of Agriculture (USDA) in the 1990s, offers the capability to quantitatively assess the structure and function of urban green spaces. It can be applied to areas of any size both urban and non-urban, thereby providing valuable insights (Nowak, 2021; Nowak and Crane, 2000; Pace et al., 2021). The model integrates various parameters such as leaf area, pollutant concentration, and dry deposition, using measurements or remote sensing. It incorporates factors such as wind speed (WS) and precipitation (PRE) and optimizes the different pollutants and vegetation characteristics, thereby ensuring highly accurate calculation results (Hirabayashi, 2011; Nowak and Crane, 2000). The model combines various parameters to simulate the physical processes of pollutant deposition, avoiding the limitations of traditional methods that rely on empirical parameters specific to different locations (Nowak et al., 2014a). To address the complexity of component interactions, Guidolotti et al. proposed the EMEP MSC-W model to reduce the dry deposition per tree and compared its results with those of the UFORE model. The comparison revealed a consistent trend between the two models, although it is worth noting that they are still limited by the fact that large-scale estimates are limited due to the availability of on-site data (Guidolotti et al., 2016).

These models undergo constant updates and iterations to keep pace with advancing technology and expanding research requirements. One major trend is their integration with other methods. For instance, the USDA has combined the dry deposition module of UFORE with a Geographic Information System (GIS) to form the i-Tree model. This model quantifies the contribution of urban green spaces by combining spatially referenced raster data from multiple sources, including atmospheric pollutants, thus overcoming the limitations of previous models that homogenize parameters such as meteorology data and pollutant concentrations (Nowak, 2021). Yin et al. utilized the UFORE to evaluate the dust retention levels of individual trees and plots in 176 urban parks. They analyzed parameters such as tree coverage, species richness, and average crown width (Yin et al., 2022). Gong et al. (2021) employed bistable isotopes and the UFORE to accurately evaluate the NO<sub>x</sub> reduction of four types of trees (*Sophora japonica*, *Fraxinus chinensis*, *Populus tomentosa*, and *Juniperus chinensis*). Their study highlighted the vital role of urban green spaces in urban development and management (Gong et al., 2021). Nowak et al. estimated air pollutant levels, including PM<sub>2.5</sub> and PM<sub>10</sub>, and the impact of dry deposits in forests and shrubs across 55 urban areas of the United States in 1994. Their findings demonstrated a total reduction of 711,000 tons with an estimated economic value of USD 3.8 billion, underscoring the irreplaceable economic and ecological value of dry deposition (Nowak et al., 2006; Nowak et al., 2018; Gong et al., 2022).

Although numerous studies have estimated the impact of dry deposition on atmospheric PM in urban green spaces (Table 1), most have relied on on-site data. Conducting continuous analyses over extended periods and at large regional spatial scales poses challenges, resulting in limited comprehensive studies being conducted on different regions in China. Hence, this study aimed to analyze the spatial and temporal changes in PM<sub>2.5</sub>, PM<sub>10</sub>, and the dry deposition effects of vegetation in China from 2000 to 2020. The analysis utilized the UFORE model, multi-source satellite remote sensing data, and wavelet coherence (WC) to investigate the relationship between multiple factors and dry deposition. The findings of this study hold significant implications for mitigating urban air pollution, guiding regional green space planning, and fostering sustainable urban development.

## 2. Material and methods

### 2.1. Study area

China is located in East Asia on the west coast of the Pacific Ocean, with a land area of approximately 9.6 million km<sup>2</sup> and a continental coastline of >18,000 km. As shown in Fig. 1, the regional vegetation in China has the following characteristics (Qin et al., 2020): 1) it is affected by the monsoon climate, and a large area of subtropical, evergreen, broad-leaved forest is distributed in the central part; 2) it spans a wide range of latitudes and longitudes; hence, the region has forests, shrubs, and alpine vegetation or aquatic and other vegetation types; and 3) it comprises unique plateau vegetation and an elevation spectrum of several peaks in the Qinghai-Tibet Plateau. The effects of vegetation cleaning on atmospheric pollutant particles were also explored in the study area. Considering the occurrence of dry vegetation deposition, only areas with tree heights above 2 m were analyzed, and the results were combined with remote sensing data products. A description of the reference data is provided in Section 2.2.

### 2.2. Experimental data

In this study, the dry deposition effect of vegetation on atmospheric PM<sub>2.5</sub> in China from 2000 to 2020 was analyzed. The model in this study involved the variables represented in green, and the trend analysis involved those represented in yellow (available at Table 2). Data were

**Table 1**  
Research status of dry deposition in urban green spaces.

Number	Method	Scale	Source citation	Limitations
1	Aerodynamics	on-site	Davidson et al. (Davidson et al., 1982)	Tailored for a specific research objective, the parameterization used in this study is inadequate, and its applicability is narrow.
2	Micrometeorology	on-site	Slinn (Slinn, 1982)	
3	ENVI-met	on-site	Bruse et al. (Bruse and Fleer, 1998; Vos et al., 2013)	When larger areas are involved, the model cannot support complex scenes and the computational effort increases.
4	UFORE	on-site	Nowak et al. (Nowak et al., 2014a; Gong et al., 2022)	
5	EMEP MSC-W	on-site	Guidolotti et al. (Guidolotti et al., 2016)	
6	UFORE + GIS (i-Tree)	Region	Zhai et al. (Zhai et al., 2022a)	Lack of research on the analysis of long-term data series.

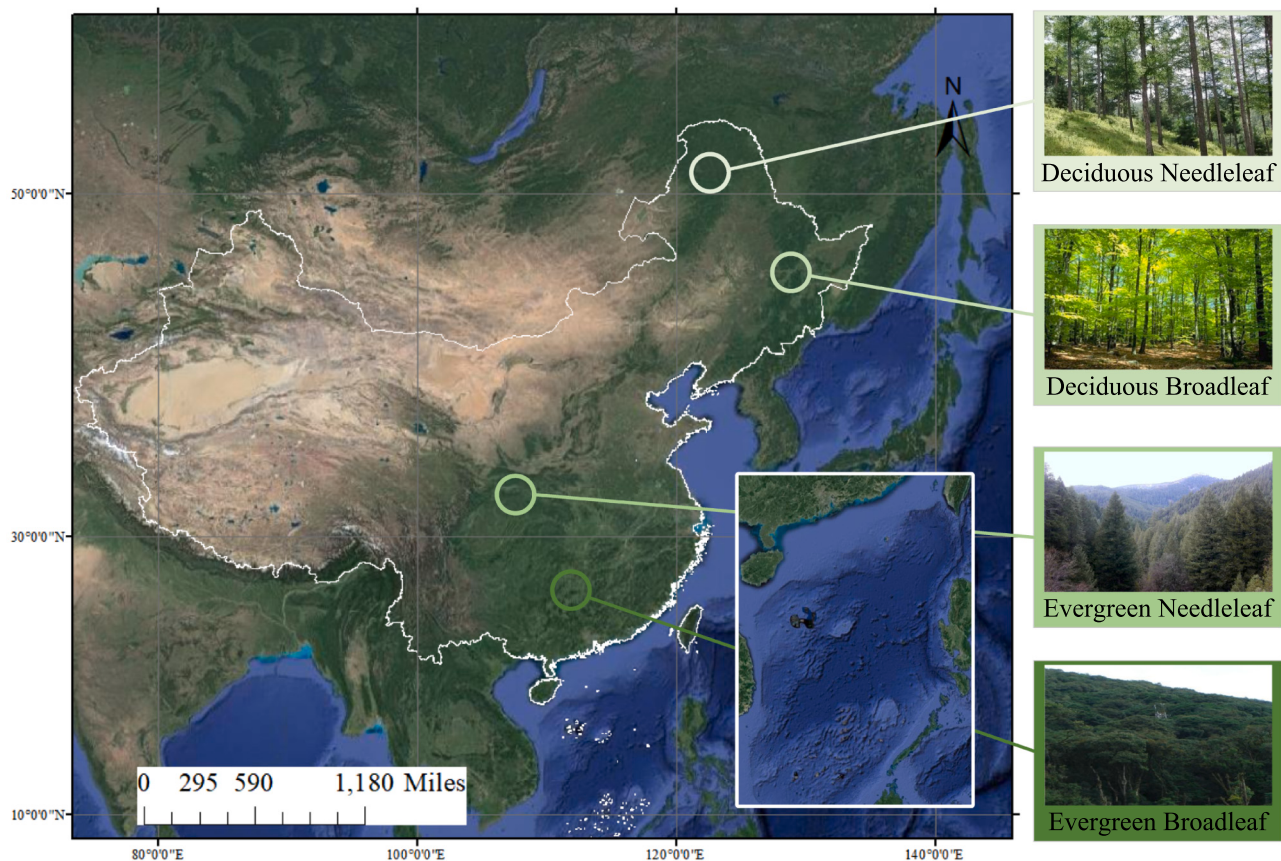


Fig. 1. Schematic diagram of the study area.

collected using the AI Earth platform, an open and free remote sensing big data platform developed by the Alibaba Damo Academy (available at <https://engine-aiearth.aliyun.com/#/>). Descriptions of each input parameter required for the estimation model are presented in Table 2. A monthly cumulative PM reduction raster dataset with a spatial resolution of 1 km was created.

#### 2.2.1. ChinaHighAirPollutants

The high-resolution and high-quality datasets of ground-level air pollutants in China (ChinaHighAirPollutants, CHAP; available at <https://weijing-rs.github.io/product.html>) contain PM, such as  $\text{PM}_{1}$  /  $\text{PM}_{2.5}$  /  $\text{PM}_{10}$ , and gaseous pollutants, such as  $\text{SO}_2$ ,  $\text{NO}_2$ , and  $\text{O}_3$ , and were produced by Wei et al. (Wei et al., 2019; Wei et al., 2021a, 2021b; Wei et al., 2022; Wei et al., 2023). Considering the spatiotemporal heterogeneity of air pollution, the dataset was generated from big data (e.g., ground measurements, satellite remote sensing products, atmospheric reanalysis, and model simulations) using an adaptive spatiotemporal artificial intelligence modeling framework. This approach addresses the challenge of missing spatial information in satellite remote sensing products and increases data availability by 60 % (Wei et al., 2023). The time coverage of the dataset is from 2000 to 2021 and includes four scales: year, month, day, and hour. In this study, monthly raster data for  $\text{PM}_{2.5}$ ,  $\text{PM}_{10}$ , and other air pollutants were used.

#### 2.2.2. ECMWF ERA5 LAND

ERA5\_LAND is a product of the European Center for Medium-Range Weather Forecasts (ECMWF) Reanalysis Program. It integrates worldwide observations over several decades into a global dataset using physical models and accurately describes past climate change (Muñoz Sabater, 2019). The dataset includes approximately 50 parameters, including temperature, PRE, albedo, soil, and snow, and provides four scales: year, month, day, and hour. Monthly grid data were used for WS,

which required preprocessing. The [ $u$  component of wind 10 m] and [ $v$  component of wind 10 m] parameters in ERA5\_LAND represent the surface 10 m wind-speed data based on the east and north. The final wind-speed data were obtained via vector synthesis in both directions.

#### 2.2.3. MOD15A2H

MOD15A2H is a MODIS L4 product that includes Leaf Area Index (LAI), Fraction of Photosynthetically Active Radiation, and corresponding quality control parameters. Its spatial resolution is 500 m and its temporal resolution is 8 days (Myneni and Park, 2021). Here, the LAI parameters were used and downsampled to a 1 km spatial resolution, and a month-scale raster dataset was used to ensure consistency with other raster datasets.

#### 2.2.4. MCD12Q1

MCD12Q1 is a MODIS L3 product that provides global landcover data in six different classifications with a spatial resolution of 500 m and a temporal scale of years (Friedl, and MCD12Q1, S.-M.D. v006, n.d.). Here, the “Land Cover Type 5: Annual Plant Functional Types” classification was used, which includes 12 categories, such as evergreen conifers (Table 3). These datasets were downsampled to a spatial resolution of 1 km to ensure consistency with the spatial resolution scales of the other raster datasets. When the dry deposition flux calculation was complete, urban green spaces (green content in Table 3) were used for mask extraction to remove interference from other feature types.

### 3. Theory

The technical route shown in Fig. 2 was used to estimate and analyze the dry deposition of atmospheric PM in urban green spaces in China from 2000 to 2020. The process could be divided into the following

**Table 2**  
Datasets used.

Number	Type	Dataset name	Temporal resolution		Spatial resolution
			resolution	Month	
1	Air pollution	China High Air Pollutants (CHAP V4) (Wei et al. 2021b)		Month	1 km
2	Wind speed	ERA5_LAND (Muñoz Sabater 2019)		Month	1 km
3	Leaf area index	MOD15A2H (Myneni and Park 2021)		Month	500 m
4	Land cover type	MCD12Q1 (Friedl and MCD12Q1)		Month	500 m
Climate Hazards Group InfraRed					
5	Precipitation	Precipitation with Station data (CHIRPS) (Funk et al. 2015)		Month	5 km
6	Normalized vegetation Index	MOD13Q1 (Didan 2015)		Month	500 m
7	Land surface temperature	MOD11A1 (Wan et al. 2015)		Month	1 km

three parts: 1) data preprocessing – vector synthesis, outlier removal, and downsampling of the original input data are required to ensure that a raster dataset with unified resolution and projection is obtained as the input data for subsequent dry deposition estimation; 2) data processing – according to the type of atmospheric pollution particles, different dry deposition estimation models are selected, and the dry deposition rate and monthly flux are estimated; and 3) data analysis – the Sen slope analysis + MK nonparametric test algorithm (MK + Sen) is used to analyze the dry deposition spatial trend followed by the WC theories to analyze the correlation between dry deposition and single- / multi-factors and to explain the dry deposition changes.

### 3.1. Estimation method of dry deposition on vegetation

This study primarily focused on the dry deposition estimation method in the UFORE model, which was used to estimate the dry deposition of pollutants, such as PM<sub>2.5</sub> and PM<sub>10</sub>, and the corresponding air quality improvement percentage within a certain time and range (Ali-Mohamed and Matter, 1996; Nowak and Crane, 2000; Ali-Mohamed, 2004; Li et al., 2014). The model was composed of multiple submodules used to quantify species composition and diversity, diameter distribution, tree density and health status, leaf area, leaf biomass, and other structural characteristics of forests. Additionally, it can be used to calculate the annual hourly volatile organic compound emissions, total carbon amounts stored each year, hourly PM removal in urban forests and their economic benefits, and the percentage of air quality improvement (Lin et al., 2021). PM reduction was defined as the cumulative time value of the product of the dry deposition flux and total area of vegetation leaves in the region. The calculation is expressed in Eq. (1):

$$R_{ij} = \sum_{i=1}^n \sum_{j=1}^m Flux_{ij} \bullet LAI_{ij} \quad (1)$$

where  $R_{ij}$  represents the annual cumulative particulate reduction (reduction) in the  $i^{th}$  row  $j^{th}$  column pixels on the grid,  $Flux_{ij}$  represents the dry deposition flux of PM per unit area, and  $LAI_{ij}$  represents the LAI mean of the current pixel obtained from the MOD15A2H product. The LAI values of each pixel were directly observed using remote sensing data. Accurate estimation of the dry deposition  $Flux$  is the key to calculating the reduction.

The dry deposition  $Flux$  represents the accumulation of PM under dry deposition per unit time and area, and is the product of the dry deposition rate and PM concentration when the total resuspended PM is simultaneously removed. This result can be obtained using Eq. (2):

$$Flux_{ij} = \sum_{i=1}^n \sum_{j=1}^m VOD_{ij} \bullet Con_{ij} \bullet t \bullet (1-s) \quad (2)$$

where  $Flux_{ij}$  represents the dry deposition flux of PM in the  $i^{th}$  row  $j^{th}$  column pixels on the grid;  $VOD_{ij}$  represents the velocity of dry deposition (VOD) on the leaf surface of the current pixel ( $m \cdot s^{-1}$ );  $Con_{ij}$  represents the concentration of PM in the current pixel (the unit is  $g \cdot m^{-3}$ , obtained from the CHAP dataset);  $t$  represents the cumulative second of the current research scale (the value in the experiment was  $30 * 24 * 60 * 60 = 2.592 * 10^6$ ); and  $s$  represents the resuspension rate of PM, which refers to the proportion of PM deposited on the leaves returning to the atmosphere and is closely related to the WS.

For vegetation, the dry deposition rate on the blade surface is defined as the reciprocal of the sum of the migration resistance of the particles from the blade surface to the interior, which is closely related to

**Table 3**  
Dataset parameters of land cover types (Friedl and MCD12Q1).

Value	Type	Description
0	Water bodies	At least 60% of area is covered by permanent water bodies
1	Evergreen needleleaf trees	Dominated by evergreen conifer trees (> 2 m); tree cover > 10%
2	Evergreen broadleaf trees	Dominated by evergreen broadleaf and palmate trees (> 2 m); tree cover > 10%
3	Deciduous needleleaf trees	Dominated by deciduous needleleaf (larch) trees (> 2 m); tree cover > 10%
4	Deciduous broadleaf trees	Dominated by deciduous broadleaf trees (> 2 m); tree cover > 10%
5	Shrub	Shrub (1–2 m) cover > 10%
6	Grass	Dominated by herbaceous annuals (< 2 m) that are not cultivated
7	Cereal croplands	Dominated by herbaceous annuals (< 2 m); at least 60% cultivated cereal crops
8	Broadleaf croplands	Dominated by herbaceous annuals (< 2 m); at least 60% cultivated broadleaf crops
9	Urban and built-up lands	At least 30% impervious surface area, including building materials, asphalt, and vehicles
10	Permanent snow and ice	At least 60% of the area is covered by snow and ice for at least 10 months of the year
11	Non-vegetated lands	At least 60% of the area is non-vegetated barren (sand, rock, or soil) with < 10% vegetation

aerodynamics, turbulent boundary layer, canopy resistance, and other variables. However, simultaneously obtaining the measured data for these variables is difficult in practical scenarios (Baldocchi et al., 1987; Nowak et al., 2008). To achieve highly automated batch processing, this definition was optimized and different methods were used to calculate the dry deposition rate  $VOD$  and resuspension rate  $s$  of  $PM_{2.5}$  and  $PM_{10}$ .

The dry deposition and resuspension rates of  $PM_{2.5}$  were greatly affected by WS. The VOD of >17 tree species has been measured under different WS conditions (Beckett et al., 2000; Frey-Smith et al., 2004; Pullman, 2008), as shown in Table 4. As the maximum hourly WS in mainland China does not exceed  $13\text{ m}\cdot\text{s}^{-1}$ , Zhai et al. established a lookup table of WS, dry deposition, and resuspension rates through nearest neighbor measurement interpolation based on previous studies. The WS range is  $1\text{--}13\text{ m}\cdot\text{s}^{-1}$  and the resolution is  $1\text{ m}\cdot\text{s}^{-1}$  (Zhai et al., 2022c). In the absence of sufficient actual observational data, the estimation accuracy of the model can be improved using this table. However, for the raster data, this table is required to provide a continuous functional relationship. Therefore, based on the lookup table, a fitting model for WS, dry deposition, and resuspension rates was constructed. The results are shown in Fig. 3.

The particle diameter of  $PM_{10}$  was much larger than that of  $PM_{2.5}$ ;

therefore, the dry deposition rate was barely affected by WS and was highly affected by tree species. Therefore, spectral indicators observed by satellite remote sensing were used to represent the differences in tree species characteristics to directly obtain the dry deposition rate change (Zhai et al., 2022a, 2022b, 2022c), as shown in Eq. (3). Because of its large particle size, the resuspension of  $PM_{10}$  was low; therefore, the resuspension rate  $s$  in Eq. (2) is 0.

$$VOD_{ij} = \sum_{i=1}^n \sum_{j=1}^m VOD_{PM_{10}} \cdot \frac{(BAI_{PM_{10}} + LAI_{ij})}{(BAI_{PM_{10}} + LAI_{PM_{10}})} \quad (3)$$

where  $VOD_{ij}$  represents the dry deposition rate of  $PM_{10}$  in the current pixel ( $\text{m}\cdot\text{s}^{-1}$ );  $VOD_{PM_{10}}$  represents the average dry deposition rate of  $PM_{10}$  under laboratory conditions, with a value of  $0.0064\text{ m}\cdot\text{s}^{-1}$ ;  $BAI_{PM_{10}}$  represents the bark area index under laboratory conditions, with a value of 1.7;  $LAI_{PM_{10}}$  represents the average measured value of LAI under laboratory conditions, with a value of 6.0; and  $LAI_{ij}$  represents the average LAI of the current pixel obtained from the MOD15A2H product. Reference measurements were obtained from a laboratory (Lovett, 1994; Tiwary et al., 2009; Zinke, 1967). After obtaining the dry deposition rates of  $PM_{2.5}$  and  $PM_{10}$ , the amount of dry deposition during the

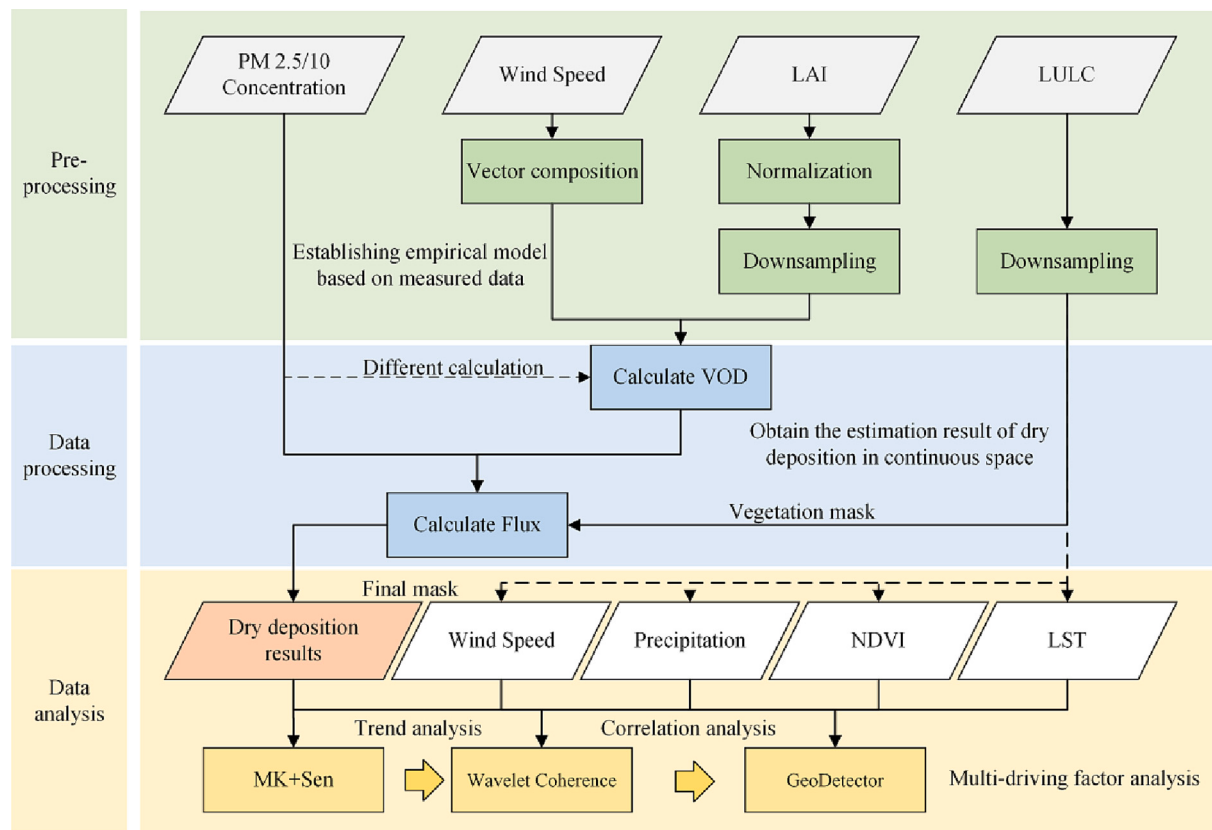


Fig. 2. Technology roadmap.

Table 4

Deposition velocity of  $\text{PM}_{2.5}$  by wind speed per unit leaf area ( $\text{m}\cdot\text{s}^{-1}$ ) (Beckett et al., 2000; Freer-Smith et al., 2004; Pullman, 2008).

Tree species	WS (Wind Speed $\text{m}\cdot\text{s}^{-1}$ )				
	1	3	6	8.5	10
<i>Quercus petraea</i>	0.00831	0.01757	0.03134		
<i>Alnus glutinosa</i>	0.00125	0.00173	0.00798		
<i>Fraxinus excelsior</i>	0.00178	0.00383	0.00725		
<i>Acer pseudoplatanus</i>	0.00042	0.00197	0.00344		
<i>Pseudotsuga menziesii</i>	0.01269	0.01604	0.0604		
<i>Eucalyptus globulus</i>	0.00018	0.00029	0.00082		
<i>Ficus nitida</i>	0.00041	0.00098	0.00234		
<i>Pinus nigra</i>	0.0013	0.0115	0.1924	0.2805	
<i>Cupressocyparis × leylandii</i>	0.0008	0.0076	0.0824	0.122	
<i>Acer campestre</i>	0.0003	0.0008	0.0046	0.0057	
<i>Sorbus intermedia</i>	0.0004	0.0039	0.0182	0.0211	
<i>Populus deltoides</i>	0.0003	0.0012	0.0105	0.0118	
<i>Pinus strobus</i>	0.000108				
<i>Tsuga canadensis</i>	0.000193				
<i>Tsuga japonica</i>	0.000058				
Maximum value of <i>Picea abies</i>	0.000189				
Minimum value of <i>Picea abies</i>	0.00038				

temporal range of the study in the experimental area was obtained using Eq. (2).

### 3.2. Wavelet coherence

In this study, we used WC to reveal the multiscale synergistic effects of multiple factors on dry vegetation deposition. The dry deposition of vegetation, PRE, land surface temperature (LST), and other factors constitute a complex nonlinear system in the time-frequency domain

scale. Multilevel-scale structures and local variation characteristics are present in this domain. Capturing these multiscale microcharacteristics can provide a deeper understanding of the influence of external environmental factors on dry vegetation deposition; however, these characteristics remain poorly understood.

The wavelet function is the focus of wavelet analysis, which refers to a class of functions with oscillating rows and can quickly decay to zero; that is, the wavelet function is  $\psi(t) \in L^2(\mathbb{R})$ , where  $\psi(t)$  is the basic wavelet function (Hu and Si, 2021). This definition is expressed in Eq. (4):

$$\psi_{a,b}(t) = |a|^{-\frac{1}{2}} \psi\left(\frac{t-b}{a}\right) \quad (4)$$

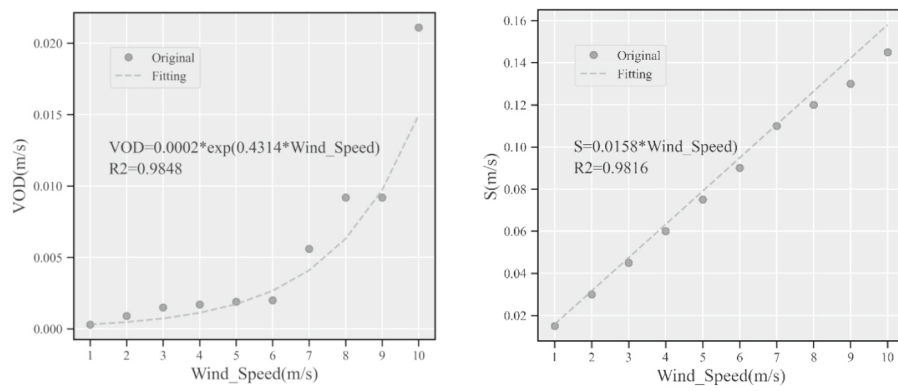
where  $\psi_{a,b}(t)$  are the subwavelets,  $a$  is the stretching scale, and  $b$  is a translation parameter. Therefore, WC in Eq. (5) is expressed as follows:

$$W_f(a, b) = |a|^{-\frac{1}{2}} \int_{\mathbb{R}} f(t) \overline{\psi}\left(\frac{t-b}{a}\right) dt \quad (5)$$

where  $W_f(a, b)$  is the WC coefficient,  $f(t)$  is a signal or square integrable function,  $a$  is the dilation scale,  $b$  is the translation parameter, and  $\overline{\psi}\left(\frac{t-b}{a}\right)$  is the complex conjugate function of  $\overline{\psi}\left(\frac{t-b}{a}\right)$ .

The WC is a combination of WC and coherence analyses. In signal analysis, a linear relationship or interdependence between variables is referred to as coherence. WC is a coefficient used to indicate the local similarity of two time series in the time-frequency domain and to determine the common change region of these series (Malakar et al., 2021), as given by Eq. (6):

$$R^2(s, \tau) = \frac{|S[s^{-1} W_{xy}(s, \tau)]|^2}{S[s^{-1} |W_x(s, \tau)|^2 \cdot s^{-1} |W_y(s, \tau)|^2]} \quad (6)$$



(a) Dry sedimentation rate fitting model

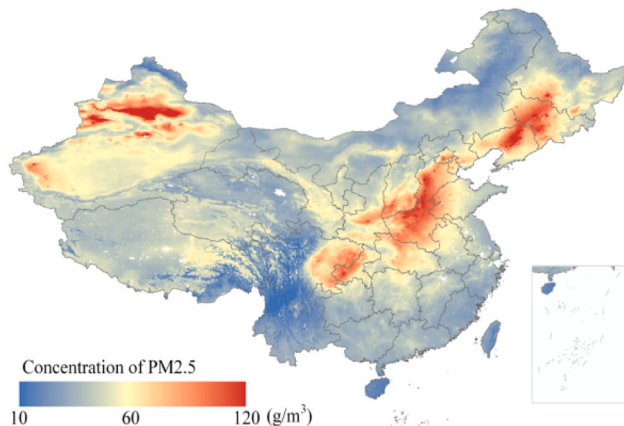
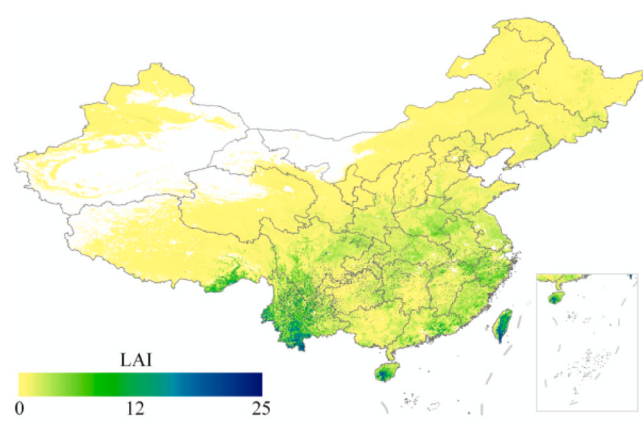
(b) Resuspension rate fitting model

**Fig. 3.** Fitting model of PM<sub>2.5</sub> dry deposition under different wind speed conditions.

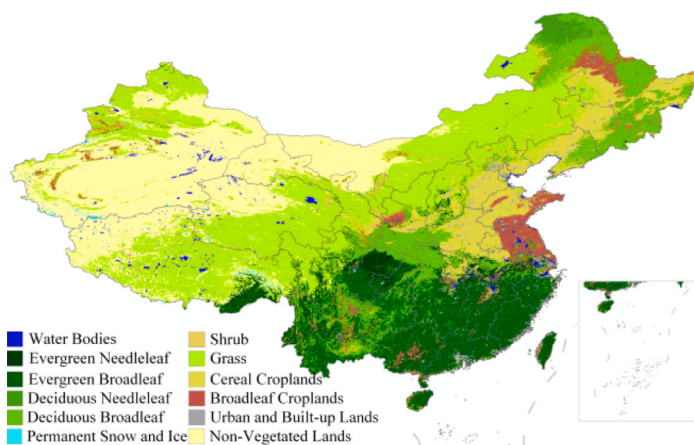
where  $s$  is the scale;  $\tau$  is the time;  $W_x(s, \tau)$  and  $W_y(s, \tau)$  are the WC of time series  $x$  and  $y$ , respectively;  $W_{xy}(s, \tau)$  is the cross WC;  $W_y(s, \tau)^*$  is the complex conjugate of  $W_y(s, \tau)$ ; and  $S$  is a smoothing operator whose definition is shown in Eq. (7):

$$S(W) = S_{\text{scale}}(S_{\text{time}}(W)) \quad (7)$$

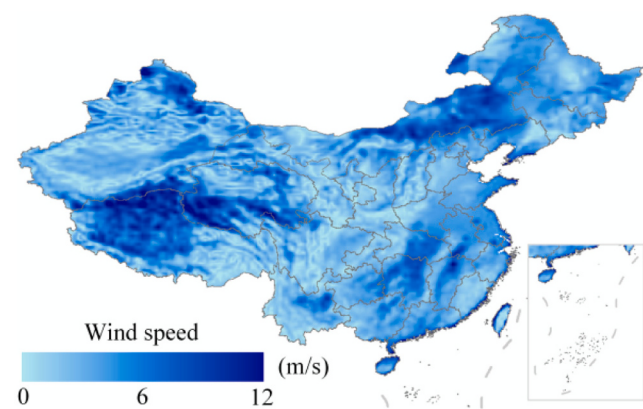
where  $S_{\text{scale}}$  and  $S_{\text{time}}$  represent the smoothing along the wavelet scale and time axes, respectively. The calculation method is expressed in Eqs.

(a) PM<sub>2.5</sub> concentration

(b) Leaf area index



(c) Land cover types



(d) Wind speed

**Fig. 4.** Spatial distribution of annual average reference data in China for the year 2000.

(8) and (9) as follows:

$$S_{time}(W)|s = \left( W_n(s) \cdot c_1^{\frac{2}{2\pi}} \right) |s \quad (8)$$

$$S_{scale}(W)|s = [W_n(s) \cdot c_2 \Pi(0.6sec)]|n \quad (9)$$

where  $c_1$  and  $c_2$  represent normalized constants,  $\Pi$  is a rectangular function, and 0.6 is the empirical value of the scale decorrelation length of the Morlet wavelet. The guiding relationship between the two time series is reflected in the wavelet phase difference (Wu et al., 2022). The wavelet phase angle between X and Y is calculated using Eq. (10):

$$\varphi(s) = \tan^{-1} (Im(W_i^{XY}(s)) / Re(W_i^{XY}(s))) \quad (10)$$

where  $Im$  and  $Re$  represent the imaginary and real parts of  $W_i^{XY}$ ,

respectively.

## 4. Results

### 4.1. Analysis of dry deposition temporal and spatial variations

The assessment of the cleaning capacity of urban green spaces in this study was related to several factors, such as air pollutant concentration, vegetation, and meteorological factors, which affect the final spatial distribution of the dry deposition flux. Regardless of the changes driven by multiple factors over the past 2 decades, these input factors have common spatial characteristics that significantly impact the results. Fig. 4 shows the spatial distribution of the input parameters for each model for the year 2000. The main sources of solid PM, such as  $PM_{2.5}$  or  $PM_{10}$ , are the byproducts of combustion and chemical manufacturing,

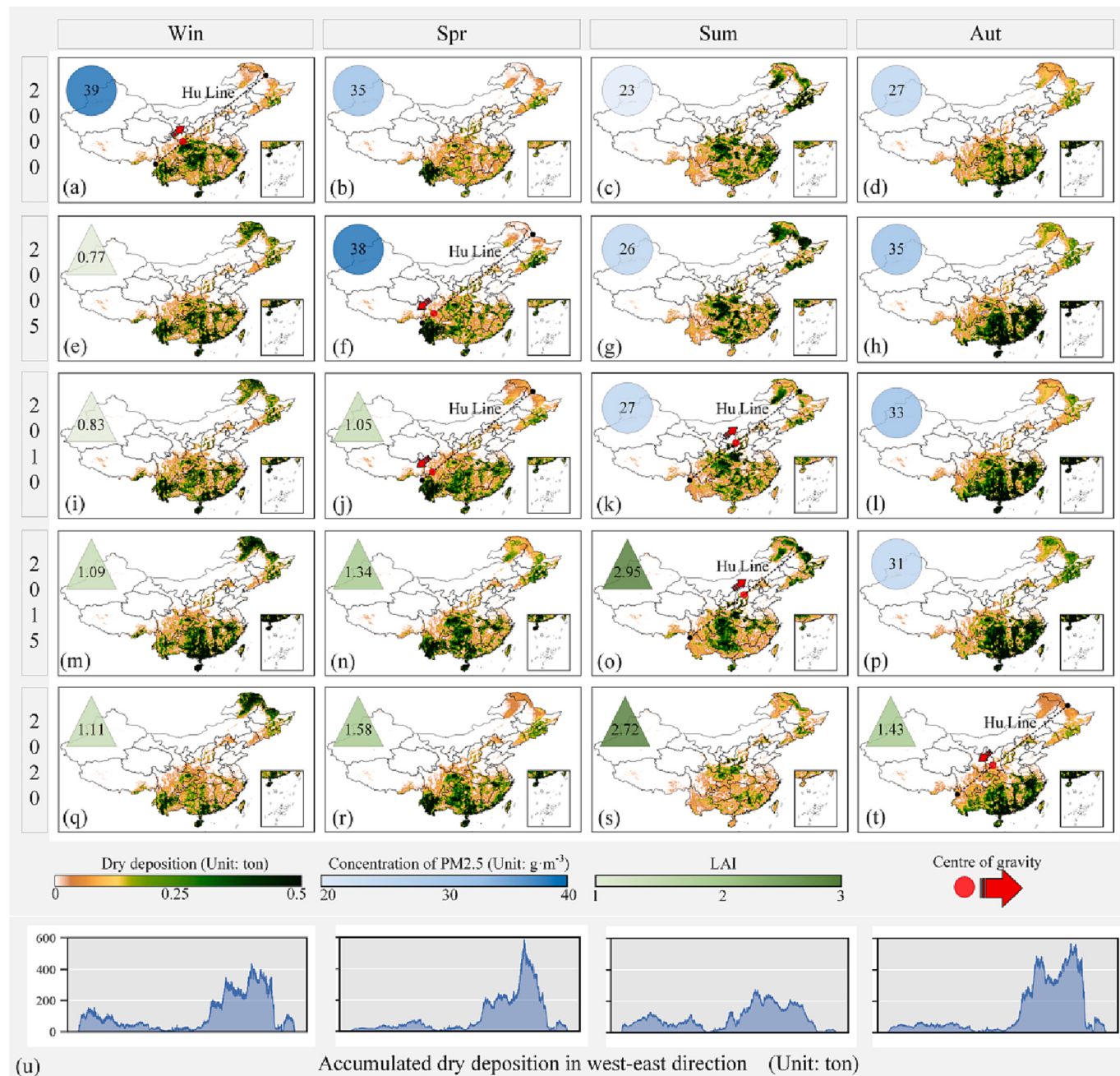


**Fig. 5.** Estimation of PM<sub>2.5</sub> dry deposition in urban green spaces in China from 2000 to 2020. (a)–(t) Spatial distribution of mean seasonal PM<sub>2.5</sub> values. (u) Corresponding to Fig. (a)–(t), the statistical curve of cumulative dry deposition in each quarter in the west-east direction.

which are strongly correlated with the development and distribution of urban industries. As shown in Fig. 4(a), central Liaoning, Beijing-Tianjin-Hebei, Urumqi, and other major heavy industrial urban agglomerations had the highest PM concentrations. These regions are followed by light industrial urban agglomerations, such as Guangdong, Hong Kong, Macao, Chengdu, and Chongqing, with distinct spatial distribution gradient changes.

Regional urban green spaces in China are primarily affected by climate change, human activity, and ecosystem evolution. China is the second-largest grassland resource country in the world, but grasslands, agricultural land, shrubs, and other vegetation do not contribute to dry deposition; therefore, they were not included in the final results. Evergreen broad-leaved, evergreen coniferous, deciduous broad-leaved, and deciduous coniferous trees (accounting for 2.65 %, 9.45 %, 3.22 %, and 9.44 % of China's overall area, respectively) play distinct roles in dry deposition. The heights of these trees are often >2 m. LAI can be used to quantify the density of vegetation leaves and canopies that play a role in removing PM per unit area. The greater the LAI value, the stronger the pollution cleaning effect. These vegetation types are mainly concentrated in northeastern and southern China (Fig. 4(b) and (c)), including *Salix babylonica*, *Platanus orientalis*, and *Cinnamomum camphora*, which have strong air purification capacities in the urban areas of China. The spatial distribution of the WS (Fig. 4(d)) is the result of meteorological and topographic factors.

The above reference data were used to form monthly grid data of dry deposition in China from 2000 to 2020. Subsequently, quarterly results were obtained by cumulative averaging based on monthly datasets. Fig. 5 shows the dry deposition estimation of PM<sub>2.5</sub> in China's urban green spaces from 2000 to 2020. The blue and green triangles represent the average PM<sub>2.5</sub> and LAI in the vegetation areas, respectively. The spatial and temporal distributions have the following characteristics: 1) seasonal variation was prominent because of the law of vegetation growth. In northern China, deciduous broad-leaved forests are dominant and the main growth season is from March to August, whereas in southern China, evergreen broad-leaved forests are dominant and the main growth season is from September to February; 2) vegetation distribution effects: owing to policy and natural conditions, northeastern and southern China have shown a notable increase in vegetation density over the years. Northeast China has been affected by the implementation of the Three-North shelter forest policy since the 1980s, whereas southern China has been affected by climatic conditions that are optimal for vegetation development (Huang et al., 2010); 3) air pollutant effects: the main sources of air pollutant emissions are industrial manufacturing byproducts and exhaust gases. China's industry is mainly distributed in the southern urban agglomeration, and the PM emissions are not limited by season and climate; thus, counter-seasonal changes are observed near factories.

Overall, the effect of vegetation on PM<sub>2.5</sub> dry deposition mainly occurred on the southeastern side of the Hu Line, which is the dividing line between China's population and economic development agglomeration, as proposed by the Chinese geographer Hu Huanyong in 1935 (Hu, 1935). This line coincides with the summer monsoon transition zone that begins and ends in Tengchong. The eastern side contains 96 % of China's population, whereas the western side contains only 4 %. However, the economic gap between the two regions is widespread. To analyze the spatial variation of dry deposition, the Hu Line was used as the axis, the cumulative amount of dry deposition was mapped to this dimension, and its center of gravity was counted, as shown by the red circle, where the corresponding arrow is the center of gravity movement trend. As shown in Fig. 5(a)–(f)–(k) and (j)–(o)–(t), from winter to autumn, the center of gravity shifted from south to north and then to south twice in the same year. The maximum annual change in a single pixel was 0.4 t, and the standard deviation of the long-term series was 0.22 t. As shown in Fig. 5(u), Fig. 5(a)–(t) is a group diagram corresponding to the west-east upward direction over many years. The cumulative dry deposition statistical curve of each quarter shows that dry

deposition mainly occurs on the southeast side of the Hu Line, and there is a center of gravity transfer with the change in season. With interannual change, dry deposition in the south shows a marked decrease, possibly related to the considerable reduction in atmospheric PM concentrations, which is discussed here in Section 4.2. In summary, the dry deposition effect of urban green spaces on PM<sub>2.5</sub> in China is extremely uneven in terms of spatial and temporal distribution. To achieve sustainable urban development, it is necessary to improve local air quality through corresponding policies.

The quarterly PM<sub>10</sub> dry deposition estimation results obtained from the monthly average raster dataset are shown in Fig. 6. The orange and green triangles represent the average PM<sub>10</sub> concentration and LAI in the vegetated area, respectively. The maximum dry deposition of PM<sub>10</sub> on a single pixel was 2 t, and the effect on improving air quality was approximately four times that of PM<sub>2.5</sub>. This may be related to the larger aerodynamic radius of PM<sub>10</sub>, which is barely affected by meteorological factors. Overall, the effect of vegetation on PM<sub>10</sub> dry deposition was high in spring and summer and low in autumn and winter, which also occurred southeast of the Hu Line. As shown in Fig. 6(a)–(f)–(k) and (j)–(o)–(t), the center of gravity shifts from north to south and then to north from winter to autumn, and fluctuates again in the same year. The maximum annual change in a single pixel is 1.8 t, and the standard deviation of the long-term series is 0.34 t, which is prominent. As shown in Fig. 6(u), the multiyear and quarterly cumulative dry deposition statistical curve of the west-east upward direction corresponding to the (a)–(t) group diagram verified the above, and no apparent center of gravity shift was observed with seasonal changes. In summary, the dry deposition of PM<sub>10</sub> in urban green spaces in China has changed dramatically in terms of spatial and temporal distribution, possibly owing to the combined action of different tree species, the external environment, and other factors.

The structure and growth period of different tree species greatly influence the dry deposition of atmospheric pollution particles, which must be included in the experimental discussion. Therefore, land cover type reference data (MCD12Q1) were introduced to calculate the cumulative dry deposition under different tree species from 2000 to 2020, as shown in Fig. 7, of which Fig. 7(a) shows the statistical results for dry deposition of PM<sub>2.5</sub> by different tree species.

The histogram in Fig. 7 corresponds to evergreen coniferous, evergreen broad-leaved, deciduous coniferous, and deciduous broad-leaved forests, with vegetation area proportions of 10.71 %, 38.13 %, 13.0 %, and 38.1 %, respectively. Compared with coniferous, larger leaf area increases the probability and total amount of dry deposition in broad-leaved, and the "roughness" of leaf surface (lots of ridges or hair) increases the intercepted surface area, but the influence of dormant season should also be considered (Sæbø et al., 2012; Yang et al., 2015). The line chart corresponds to the cumulative value of annual dry deposition. Overall, from 2000 to 2013, the dry deposition effects of PM<sub>2.5</sub> and PM<sub>10</sub> on vegetation showed fluctuating, with the reduction of PM<sub>2.5</sub> and PM<sub>10</sub> increasing from  $0.83 \times 10^6$  to  $1.43 \times 10^6$  t and from  $3.53 \times 10^7$  to  $5.45 \times 10^7$  t, respectively. From 2013 to 2020, this effect showed a linear decreasing trend with the reduction of PM<sub>2.5</sub> and PM<sub>10</sub> from  $1.43 \times 10^6$  to  $0.75 \times 10^6$  t and from  $5.45 \times 10^7$  to  $2.91 \times 10^7$  t, respectively. The year 2013 was the key inflection point for the change in dry deposition because China launched the "Air Pollution Prevention and Control Action Plan" that year, after realizing the harmful effects of air pollution, calling for energy conservation and emission reduction in major urban agglomerations to reduce the overall atmospheric PM concentration by 10 % (Wang et al., 2019). Subsequently, the concentration of atmospheric pollution particles decreased substantially, affecting the cleaning of urban green spaces. The statistical results showed that dry deposition in 2020 was even lower than that in 2000.

The overall effects of dry deposition varied drastically among the different tree species. In 2013, the annual dry deposition of PM<sub>2.5</sub> in China was ranked as follows: evergreen broadleaf ( $0.83 \times 10^6$ , 58.14 %) > deciduous broadleaf ( $0.44 \times 10^6$ , 31.08 %) > evergreen needleleaf

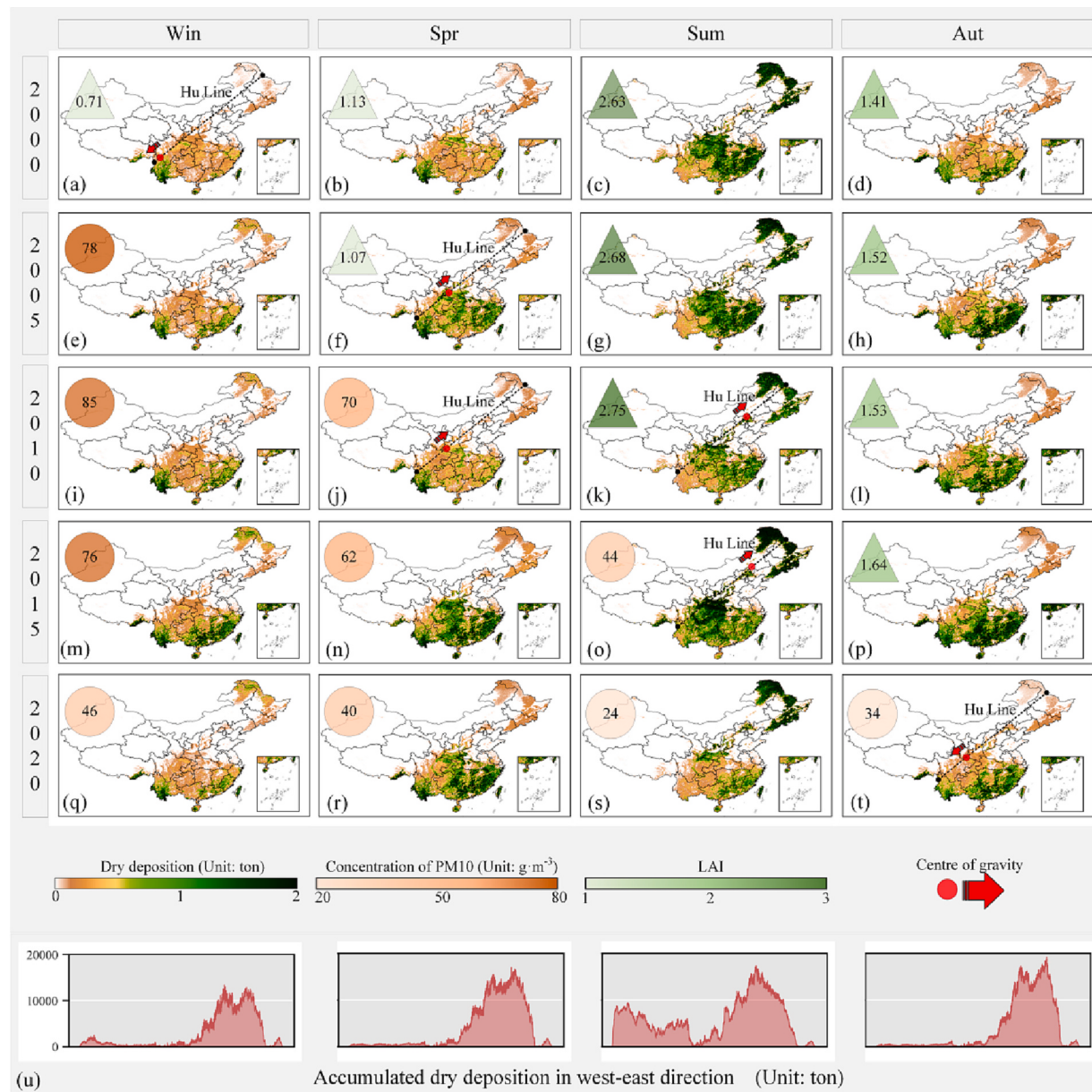


**Fig. 6.** Spatial distribution of PM<sub>10</sub> dry deposition estimated for urban green spaces in China. (a)–(t) Spatial distribution of the mean value of PM<sub>10</sub> dry deposition. (u) Corresponding to Fig. (a)–(t), the statistical curve of cumulative dry deposition in each quarter in the west-east direction.

( $0.13 * 10^6$ , 9.03 %)  $>$  deciduous needleleaf ( $0.02 * 10^6$ , 1.73 %). In subsequent years, the proportion of dry deposition for each tree species did not significantly differ from that in 2013. In China, the main vegetation type is broad-leaved forests, which account for 76.24 % of the total vegetation area and 89.22 % of the total dry deposition, which is approximately nine times that of coniferous forests. Although the area of evergreen broad-leaved forests is approximately equal to that of coniferous broad-leaved forests, the total amount of dry deposition in evergreen broad-leaved forests is twice that of coniferous broad-leaved forests. This observation indicates that the dry deposition rate and the effects of evergreen broad-leaved forests on PM<sub>2.5</sub> and PM<sub>10</sub> were the highest. In subsequent urban development planning, the density of evergreen broad-leaved trees should be appropriately increased in combination with appropriate climate and geographical conditions to improve air quality.

Although afforestation and enhanced green density are important means of preventing and controlling air pollution in Chengdu, forests have limitations in improving the atmospheric environment. However,

solving the fundamental problem of air pollution is challenging. In Fig. 7 (a) and (b), dry deposition shows a rapid decline after 2013, which was not due to significant changes in vegetation or meteorological conditions; however, the concentration of atmospheric pollutants decreased sharply owing to local policies. As shown in Table 5, this observation is based on the statistical results of the CHAP dataset and those of this study. From 2000 to 2013, PM<sub>2.5</sub> and PM<sub>10</sub> concentrations increased at a rate of approximately 10 % per year and peaked in 2013. From 2013 to 2020, these concentrations began to decline at a rate of approximately 15 % annually, reaching a minimum in 2020. Combined with the results from Fig. 7, the overall trend of dry deposition fluctuated around the change in atmospheric PM concentration, indicating that the dominant factor affecting the change in dry deposition was the concentration of atmospheric PM. The key to alleviating air pollution is controlling emission sources and reducing pollutant emissions. The cleaning effect of urban green spaces on air pollutants is the result of several factors, and it is necessary to analyze the influence of a single variable on complex results.

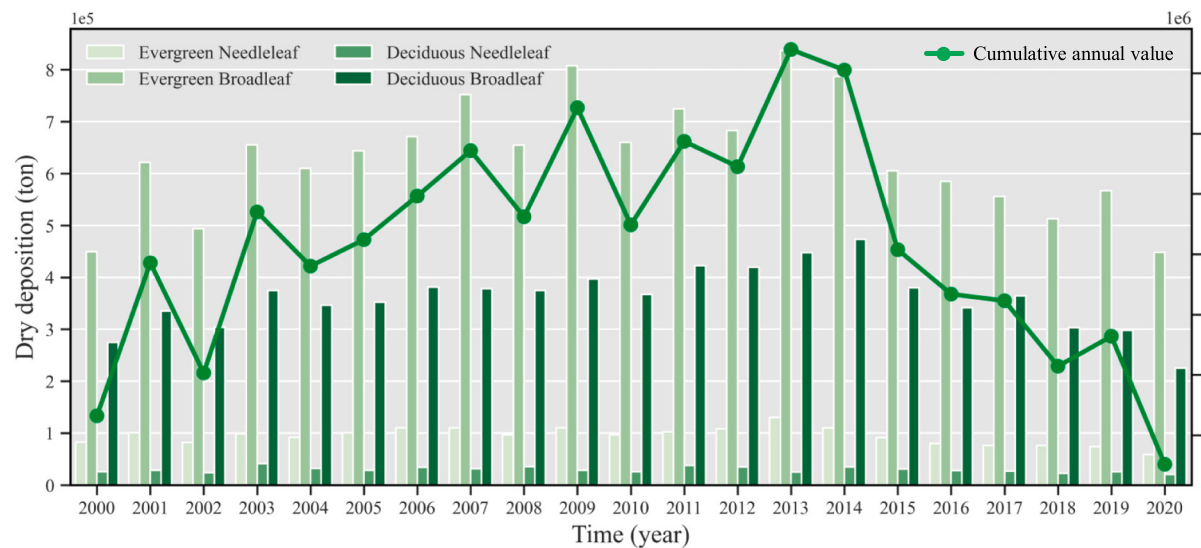
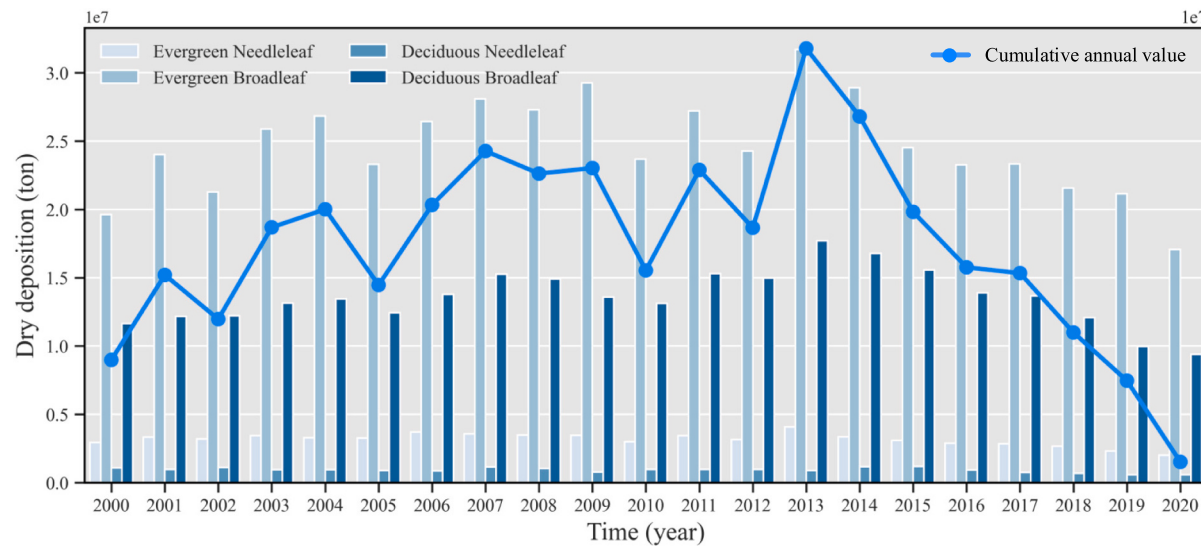
(a) Analysis of dry deposition of PM<sub>2.5</sub> by different tree species(b) Analysis of dry deposition of PM<sub>10</sub> by different tree species

Fig. 7. Analysis of dry deposition changes of different tree species from 2000 to 2020.

#### 4.2. Multi-driving factors analysis of dry deposition

Urban green spaces provide ecological protection and restoration services for urban development, with dry vegetation deposition as the main contributor. Dry deposition is a process in which suspended particles migrate from the lower atmosphere to the underlying surface via gravity, interception, and adsorption. The dry deposition of PM<sub>2.5</sub> & PM<sub>10</sub> on vegetation is related to several factors, such as vegetation growth status and the external environment. Based on wavelet and

multi-WCs methods, we tried to explore the correlation between the dry deposition and environmental factors, such as WS, PRE, normalized difference vegetation index (NDVI), and LST. After the above calculation, the obtained WC value was between zero and one, which was similar to that of the Pearson correlation coefficient. This value can be regarded as the local correlation coefficient in time-frequency space. The larger the value, the stronger the correlation. In the wavelet analysis, a 95 % confidence level was obtained using a Monte Carlo repeat based on the first-order autocorrelation coefficient (1000 repeats). As

**Table 5**  
Analysis of the influence of dry deposition in urban green spaces.

Year	2000	2005	2010	2013	2015	2020
Concentration of PM <sub>2.5</sub> / (g·m <sup>-3</sup> )	32	37	38	40	33	21
Concentration of PM <sub>10</sub> / (g·m <sup>-3</sup> )	57	63	65	68	57	36
Dry deposition of PM <sub>2.5</sub> / (10 <sup>3</sup> t)	832	1124	1148	1439	1107	751
Dry deposition of PM <sub>10</sub> / (10 <sup>3</sup> t)	35275	39873	40769	54385	44361	29021

\*Orange: increase from the previous year; blue: decrease from the previous year.

wavelet analysis is applied to limited time-series data, an edge effect may occur at the edge of the time series. Therefore, the region related to the edge effect is defined as the influence cone (COI), and the wavelet power within the COI cannot be estimated reliably. The explanatory power of the predictors of the response variables was quantitatively evaluated by calculating the proportions of areas of significant coherence (PASC) and average WC (AWC).

Fig. 8 shows the local changes in PM<sub>2.5</sub> and PM<sub>10</sub> as well as the coherence of each influencing factor during the study period. PM<sub>2.5</sub> and WS had significant interannual and interdecadal oscillation modes. On the high-frequency scale (32 months), the cross-phase angle between PM<sub>2.5</sub> and WS was approximately 90° upward, PM<sub>2.5</sub> delayed WS by

approximately 1 / 4 period, and the coherence between PM<sub>2.5</sub> and WS was greater on the low-frequency scale than on the high-frequency scale. The significant resonance period of PM<sub>2.5</sub> and PRE was mainly concentrated on the 8–16 month scale, the cross-phase angle was upward, PM<sub>2.5</sub> delayed PRE by approximately 1 / 4 period, and at the high-frequency scale (< 8 months), PM<sub>2.5</sub> had a significantly negative correlation with PRE. The cross-phase angle of PM<sub>2.5</sub> and NDVI changed irregularly on the <8 month scale. At the 8–16 month scale, the cross-phase angle between PM<sub>2.5</sub> and NDVI was approximately 90° upward, and PM<sub>2.5</sub> delayed NDVI by approximately 1 / 4 cycles. At the 16 month scale, coherence was not apparent. On the high-frequency scale, PM<sub>2.5</sub> and LST had significant and dispersed positive-phase resonance periods

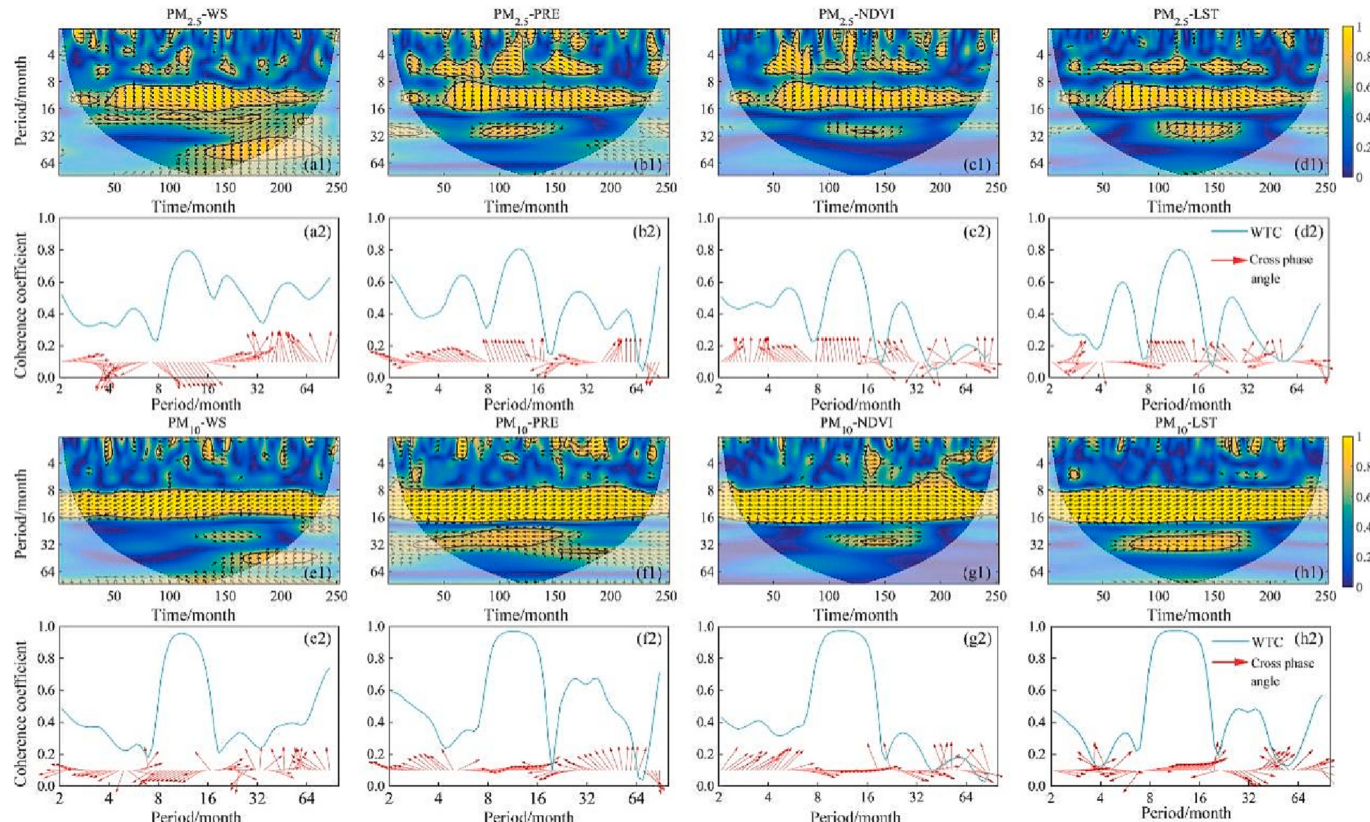


**Fig. 8.** PM<sub>2.5</sub> and PM<sub>10</sub> WC analysis results. The arrow indicates the relative phase difference, → same phase, ← opposite phase, ↑ PM<sub>2.5</sub> and PM<sub>10</sub> are delayed in the impact factor, and ↓ PM<sub>2.5</sub> and PM<sub>10</sub> are ahead of the impact factor. The black solid line indicates a 95 % confidence level red noise test, and the shadow area is the wavelet influence cone (COI).

only on the 4–8 month scale, indicating that PM<sub>2.5</sub> and LST have consistent changes on this scale, but significant coherence is rarely observed on the <4 month scale. On the 8–16 month scale, the cross-phase angle between PM<sub>2.5</sub> and LST was upward, and PM<sub>2.5</sub> delayed LST by approximately 1 / 2.

The significant correlation domains between PM<sub>10</sub> and the impact factors were mainly concentrated on the 8–16 month scale. On this scale, PM<sub>10</sub> was significantly negatively correlated with the WS and significantly positively correlated with the PRE, NDVI, and LST. At the high-frequency scale (16 month scale), the coherence domain of PM<sub>10</sub> with WS and NDVI was not significant and was partially affected by the wavelet-edge effect. PM<sub>10</sub> was significantly negatively correlated with PRE and significantly positively correlated with LST. The high coherence between PM<sub>10</sub> and the impact factors was also mainly concentrated on the 8–16 month scale. The coherence between PM<sub>10</sub> and WS at the high-frequency scale was greater than that at the low-frequency scale, whereas the coherence between PM<sub>10</sub> and PRE, NDVI, and LST at the high-frequency scale was lower than that at the low-frequency scale.

The statistical results corresponding to Fig. 8 are listed in Table 6. Generally, the coherence of PM<sub>2.5</sub> and each impact factor in the time domain is more complex than that of PM<sub>10</sub>, and the high coherence domains of PM<sub>2.5</sub>, PM<sub>10</sub>, and the impact factor are mainly concentrated on the 8–16 month scale. At this scale, the significant coherence domain of PM<sub>10</sub> and the impact factor covered the entire study period, whereas that of PM<sub>2.5</sub> and the impact factor were not completely covered. NDVI is an important parameter affected by dust retention in green spaces. The more complex the vertical structure of the green space, the higher the dust retention effect. LST affects the Brownian diffusion and gravity deposition processes of the particles. The higher the temperature, the more intense the Brownian motion and the greater the gravitational deposition rate. The LST accelerates photochemical reactions and pollutant formation. PRE can cause hygroscopic particles to swell and increase the viscosity of the plant surface, thereby accelerating deposition, reducing the resuspension of particles, and affecting vegetation porosity, thus, affecting the dust retention rate. The WC statistical results (Table 6) suggest that the PRE dominantly affected PM<sub>2.5</sub> and PM<sub>10</sub> (with the highest PASC), whereas LST and WS had the least correlation with PM<sub>2.5</sub> and PM<sub>10</sub>, respectively.

Table 6 shows that the coherence between PM<sub>2.5</sub> and a single impact factor was not significant when compared with PM<sub>10</sub>. Therefore, a multi-WC model was introduced to analyze the relationship between PM<sub>2.5</sub> and multiple impact factor combinations (Fig. 9). Compared to WC, the multi-WC model can analyze the synergistic effects of multiple factors on PM<sub>2.5</sub> reduction at multiple scales. Distinct periodic gradient changes were present between the two-factor combination and the three- and four-factor combinations, and the response ability of different combinations to the change in the reduction amount was different at different time-frequency scales. On an hourly scale, the best bivariate combination to explain the change in PM<sub>2.5</sub> reduction was WS-PRE, and the best three-variable combination was WS-PRE-NDVI. On the medium time-frequency scale, the best bivariate combination to explain this phenomenon was PRE-LST, and the best three-variable combination was WS-PRE-LST. On a large time-frequency scale, the best bivariate

combination to explain this change was PRE-NDVI, and the best three-variable combination was WS-PRE-NDVI.

From Table 7 and the quantitative statistical results corresponding to Fig. 9, it was determined that on different time-frequency scales, the combination of each influencing factor was roughly similar to the PASC.

These results were different for the AWC. The best bivariate combination for explaining PM<sub>2.5</sub> was WS-PRE (PASC = 22.91 %, AWC = 0.74), and the best three-variable combination was WS-PRE-NDVI (PASC = 18.74 %, AWC = 0.85). Compared with a single impact factor, the combination of impact factors improved the understanding of changes in PM<sub>2.5</sub> on an hourly frequency scale. Additionally, AWC increased with an increase in the number of predictors; however, PASC did not necessarily increase. For example, the PASC of the three-variable combination was smaller than that of the two-variable combination, possibly for the following reasons: 1) additional variables lead to a simultaneous increase in the significance threshold, and 2) the significant coherence domains of multiple predictors and response variables overlap, and the collinearity effect between predictors reduces the predictor variance contribution rate. Therefore, the explanatory power of variable combinations on changes in PM<sub>2.5</sub> is significantly improved by adding predictive variables that can independently explain these changes at a specific scale. However, this finding also confirms the limitations of environmental factors in reducing atmospheric PM, and that concentration changes may occupy a greater weight in the results.

## 5. Discussion

The removal of atmospheric pollutants by urban green spaces has been widely studied; however, some differences remain in the estimation methods and application scenarios (Nowak and Crane, 2000; Nowak et al., 2014a; Zhai et al., 2022c). Dry deposition in urban green spaces is affected by numerous factors, such as vegetation characteristics, environmental factors, and human activities, as well as variables used in the UFORE model, such as changes in the atmospheric boundary layer height, indicating that this model still has room for improvement (Nowak et al., 2014b; Whitlow et al., 2014). Additionally, according to different application scenarios, the research scale can be as large as urban agglomerations or as small as individual trees, and different research scales must consider these influences in greater detail (Gong et al., 2021; Lin et al., 2021). Compared with existing research, this study has notable differences in research scale in that a large area, such as China, was used as the research object, and the point data of ground observation stations were replaced with the area data of satellite remote sensing observations. Because of these differences, the original algorithm of the UFORE model was improved by ignoring the influence of the daily PRE frequency on the resuspension rate in the estimation of the annual cumulative dry deposition.

### 5.1. Analysis of spatial and temporal variation trends in vegetation dry deposition

In Section 4.1, using the UFORE model, the dry deposition of vegetation was quantified from 2000 to 2020 and its changing characteristics were analyzed from the two dimensions of space and time. It was found that the dry deposition of vegetation is the product of a variety of factors and that there is a complex interaction between these factors, which, in turn, affects the final estimation accuracy of the model, where atmospheric PM concentrations and tree species may be the two main influencing factors.

Based on this preliminary conclusion, and to analyze the spatial and temporal variation trends in the long-term series of vegetation dry deposition, the MK + Sen nonparametric test algorithm was used, which has been successfully applied in studies of hydrological and meteorological trend changes. This study implemented an algorithm using a third-party open-source library (Hussain and Mahmud, 2019). First, a long-term sequence raster dataset was sent to the Sen module for trend

**Table 6**

Parameter statistics of WC between PM<sub>2.5</sub> and PM<sub>10</sub> and various influencing factors.

WC	PASC (%)	AWC
PM <sub>2.5</sub> -WS	21.97	0.50
PM <sub>2.5</sub> -PRE	25.57	0.49
PM <sub>2.5</sub> -NDVI	21.40	0.44
PM <sub>2.5</sub> -LST	19.04	0.40
PM <sub>10</sub> -WS	22.76	0.44
PM <sub>10</sub> -PRE	35.63	0.57
PM <sub>10</sub> -NDVI	31.36	0.50
PM <sub>10</sub> -LST	32.56	0.51

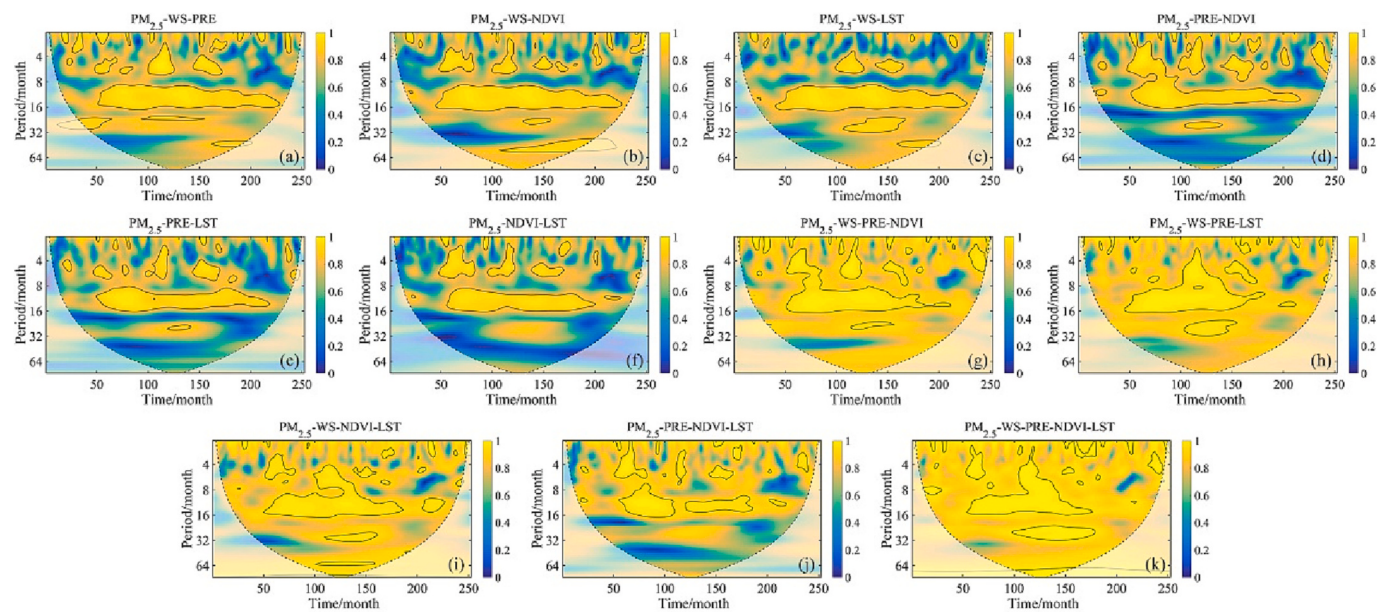


**Fig. 9.** Results of multi-WC analysis of  $\text{PM}_{2.5}$  and multi-impact factors combination.

**Table 7**

Parameter statistics of multi-WC between  $\text{PM}_{2.5}$  and  $\text{PM}_{10}$  and various influencing factors.

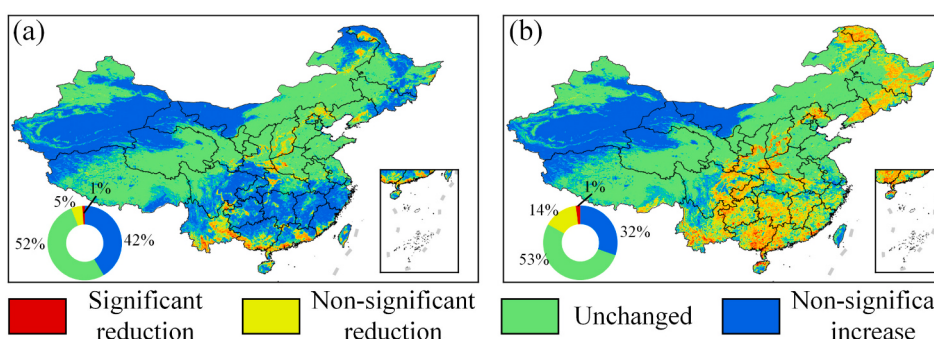
Combinations	PASC (%)	AWC
Two factors	PM <sub>2.5</sub> -WS-PRE	22.91
	PM <sub>2.5</sub> -WS-NDVI	22.02
	PM <sub>2.5</sub> -WS-LST	19.62
	PM <sub>2.5</sub> -PRE-NDVI	20.78
	PM <sub>2.5</sub> -PRE-LST	15.31
Three factors	PM <sub>2.5</sub> -NDVI-LST	15.37
	PM <sub>2.5</sub> -WS-PRE-NDVI	18.74
	PM <sub>2.5</sub> -WS-PRE-LST	18.31
	PM <sub>2.5</sub> -WS-NDVI-LST	17.89
	PM <sub>2.5</sub> -PRE-NDVI-LST	12.46
Four factors	PM <sub>2.5</sub> -WS-PRE-NDVI-LST	19.37

analysis. Second, the dataset was sent to the MK module for significance testing and combined with the output results of the two modules. The trend results were obtained via reclassification and reanalysis, as shown in Fig. 10. In China, there was no significant change in the cleaning effect of urban green spaces on  $\text{PM}_{2.5}$ , and only a few urban communities exhibited a significant decrease (Fig. 10(a)). The cleaning effect of urban green spaces on  $\text{PM}_{10}$  changed dramatically and decreased significantly

in northeastern and southern China (Fig. 10(b)). Compared with  $\text{PM}_{2.5}$ , the cleaning effect of urban green spaces on  $\text{PM}_{10}$  changes was more noticeable, with 10 % more pixels showing an increasing trend. This result may be related to the decrease in PM concentrations in air pollution; however, the effect of vegetation on  $\text{PM}_{10}$  was weaker than that on  $\text{PM}_{2.5}$ .

### 5.2. Response of vegetation dry deposition to environmental factors

In Section 4.2, multi-WC was used to analyze the period and coherence between vegetation dry deposition and multiple factors; however, the local characteristics and macro-relationship of the signal in the time domain could not be extracted. Therefore, GeoDetector was introduced as a supplement to WC and to verify the global features. Geodetectors are geographical models used to analyze complex phenomena under multifactor interactions (Wang and Xu, 2017). This model was used to analyze the contribution of multiple factors to dry deposition as a supplement and side confirmation of WC. First, according to the requirements of the geographic detector for the data type of driving factors, the natural breakpoint method was used to divide the monthly average WS, monthly cumulative PRE, and monthly average LST into six categories, and the monthly maximum synthetic NDVI was divided into four categories. Next, the factor and interaction detection of  $\text{PM}_{2.5}$  and



(a) Cleaning effect of urban green spaces on  $\text{PM}_{2.5}$  (b) Cleaning effect of urban green spaces on  $\text{PM}_{10}$

**Fig. 10.** Trend analysis of dry deposition of urban green space vegetation in China from 2000 to 2020.

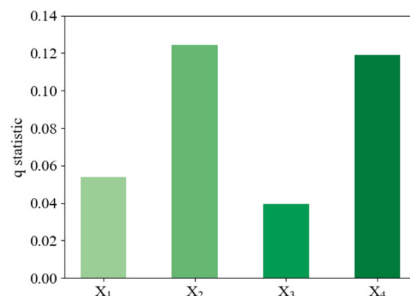
$\text{PM}_{10}$  was conducted using a geographic detector, and the results are shown in Fig. 11.

For  $\text{PM}_{2.5}$ , the explanatory power of each driving factor was ranked as follows: monthly cumulative PRE > monthly average LST > monthly average WS > monthly maximum synthetic NDVI (Fig. 11(a)). The significance levels of the monthly cumulative PRE, monthly average LST, and monthly maximum synthetic NDVI were above 95 %. The monthly cumulative PRE and monthly average LST had strong explanatory powers, reaching 0.124 and 0.119, respectively, indicating that they are important factors affecting  $\text{PM}_{2.5}$ . For  $\text{PM}_{10}$  reduction, the explanatory power of each driving factor was ranked as follows: monthly average LST > monthly maximum synthetic NDVI > monthly cumulative PRE > monthly average WS, with significance levels above 99 % (Fig. 11(b)). The monthly average LST and monthly maximum composite NDVI had values >0.59, indicating a significant impact on  $\text{PM}_{10}$  reduction. The detection results of the spatial differentiation interaction between  $\text{PM}_{2.5}$  and  $\text{PM}_{10}$  reduction are shown in Fig. 11(c) and (d), where the interaction explanatory power of any two driving factors is greater than that of a single driving factor. The interaction between factors has a two-factor enhancement and nonlinear enhancement trend for the reduction of  $\text{PM}_{2.5}$  and  $\text{PM}_{10}$ . Coupling different factors increases the explanatory power of  $\text{PM}_{2.5}$  and  $\text{PM}_{10}$  reductions. The monthly cumulative PRE  $\cap$  monthly maximum composite NDVI has the strongest explanatory power of 0.666, indicating that the combined effect of the two has a significant impact on  $\text{PM}_{10}$  reduction. Comparing the interactive driving results of  $\text{PM}_{2.5}$  and  $\text{PM}_{10}$  reductions, the interaction between the monthly average WS and the other factors was higher for both dependent variables, indicating that the monthly average WS is one of the key factors affecting air quality.

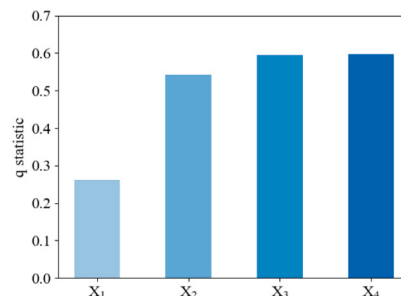
## 6. Conclusions

Based on the UFORE algorithm, this study overcame the limitations of traditional site-scale research by combining multi-source satellite remote sensing products to form a dry deposition estimation raster dataset of  $\text{PM}_{2.5}$  and  $\text{PM}_{10}$  for China's urban green spaces from 2000 to 2020. Additionally, the spatio-temporal changes in the long-term series were analyzed and wavelet coherence was combined to analyze the impact of environmental factors on dry deposition, thus providing a scientific reference and theoretical basis for better understanding the ecological and environmental benefits of vegetation. The resulting conclusions are as follows:

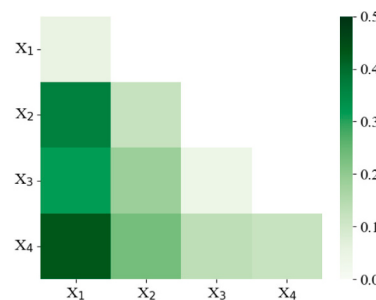
1. The dry deposition in urban green spaces mainly occurred on the southeastern side of the Hu Line. The north of the Hu Line focuses on the Three North Shelterbelts, whereas the south focuses on the metropolitan group. The overall center of gravity migrated twice from winter to autumn, and at the maximum dry deposition per pixel,  $\text{PM}_{10}$  was approximately four times that of  $\text{PM}_{2.5}$ .
2. The main source of dry deposition in urban green spaces in China is broad-leaved forests, accounting for 76.24 % of the total vegetation area and 89.22 % of the total dry deposition; the dry deposition on evergreen broad-leaved trees per unit area is twice that of deciduous broad-leaved trees. In subsequent urban development planning, the density of evergreen broad-leaved trees should be appropriately increased in combination with appropriate climate and geographical conditions to improve air quality.
3. PM have typical time-frequency scale coherence with environmental factors. The WC results showed that the significant coherence domains of PM and environmental factors were concentrated from 8 to 16 months, but the coherence between  $\text{PM}_{2.5}$  reduction and environmental factors in the time domain space was more complex than



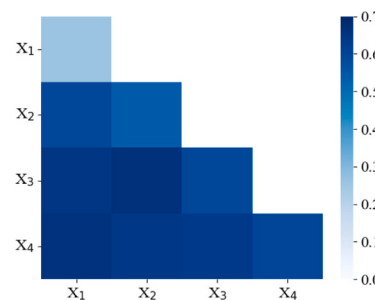
(a)  $\text{PM}_{2.5}$  factor detection results



(b)  $\text{PM}_{10}$  factor detection results



(c)  $\text{PM}_{2.5}$  interaction detection results



(d)  $\text{PM}_{10}$  interaction detection results

**Fig. 11.** Geodetector analysis results.  $X_1$ : monthly average wind speed;  $X_2$ : monthly cumulative precipitation;  $X_3$ : maximum monthly composite normalized difference vegetation index (NDVI); and  $X_4$ : monthly mean land surface temperature (LST).

that of PM<sub>10</sub>. The precipitation predominantly explained the changes in PM<sub>2.5</sub> and PM<sub>10</sub>, while land surface temperature and wind speed had the least correlation.

However, some limitations remain, such as the need to introduce more measured data to improve the settlement rate-fitting model. These limitations will be the main focus of our further research. The current and subsequent versions of the Dry Deposition Effect of urban green spaces on ambient Pollution in China (DDEP) dataset will be available on AI Earth (URL: [https://engine-aiearth.aliyun.com/#/data-set/TJNU\\_3JEQO\\_CHINA\\_DDEP\\_V01](https://engine-aiearth.aliyun.com/#/data-set/TJNU_3JEQO_CHINA_DDEP_V01)).

## Author contributions statement

Jiaqi Yao proposed the methodology and wrote the manuscript. Shuqi Wu and Yongqiang Cao contributed to improving the methodology and is the corresponding author. Jing Wei, Xinming Tang, Liuru Hu and Jianjun Wu helped edit and improve the manuscript. Huicai Yang, Jianhua Yang and Xinhui Ji contributed to methodological testing. All authors have read and agreed to the published version of the manuscript.

## Role of the funding source

This work was supported by the National Natural Science Foundation of China [grant number 52079060]; the Belt and Road Initiative Water and Sustainable Development Science and Technology Key Fund [grant number 2021nkzd02], and the Special Funds for Creative Research [grant number 2022C61540].

## Declaration of competing interest

The authors declare that they have no known competing financial interests or personal relationships that could have appeared to influence the work reported in this paper.

## Data availability

Data will be made available on request.

## References

- Ali-Mohamed, A.Y., 2004. Inorganic chemical composition of aerosols settling in Hamad Town, Bahrain following dust haze storms. *Int. J. Environ. Stud.* 61 (2), 161–171.
- Ali-Mohamed, A.Y., Matter, H.A., 1996. Determination of inorganic particulates: (cationic, anionic and heavy metals) in the atmosphere of some areas in Bahrain during the Gulf crisis in 1991. *Atmos. Environ.* 30 (20), 3497–3503.
- Baldocchi, D.D., Hicks, B.B., Camara, P., 1987. A canopy stomatal resistance model for gaseous deposition to vegetated surfaces. *Atmos. Environ.* 21, 91–101.
- Beckett, K.P., Freer-Smith, P., Taylor, G., 1998. Urban woodlands: their role in reducing the effects of particulate pollution. *Environ. Pollut.* 99, 347–360.
- Beckett, K.P., Freer-Smith, P., Taylor, G., 2000. Particulate pollution capture by urban trees: effect of species and windspeed. *Glob. Chang. Biol.* 6, 995–1003.
- Bruse, M., Fleer, H., 1998. Simulating surface-plant-air interactions inside urban environments with a three dimensional numerical model. *Environ. Model. Softw.* 13 (3/4), 373–384.
- Chen, X., Jiao, Y., Pei, T., Zhou, Z., 2014. The effect of adsorbing fine particulate matter (PM<sub>2.5</sub>) by garden plants: a review. *Chin. J. Ecol.* 33, 2558–2566.
- Davidson, C.I., Miller, J.M., Pleskow, M.A., 1982. The influence of surface structure on predicted particle dry deposition to natural grass canopies. *Long-Range Transport of Airborne Pollutants.* 25–43.
- DeJarnett, N., McDonald, R., McDonald, R., 2016. Planting healthier air: an assessment of the potential for trees to reduce air pollution and cool cities to enhance human health. In: APHA 2016 Annual Meeting & Expo.
- Dominici, F., Greenstone, M., Sunstein, C.R., 2014. Particulate matter matters. *Science* 344 (6181), 257–259.
- Fan, S., Yan, H., Qi, S., Bai, W., Pi, D., Li, X., Dong, L., 2015. Dust capturing capacities of twenty-six deciduous broad-leaved trees in Beijing. *Chin. J. Plant Ecol.* 39, 736–745.
- Freer-Smith, P., El-Khatib, A., Taylor, G., 2004. Capture of particulate pollution by trees: a comparison of species typical of semi-arid areas (*Ficus nitida* and *Eucalyptus globulus*) with European and north American species. *Water Air Soil Pollut.* 155, 173–187.
- Friedl, M., MCD12Q1, S.-M.D. v006. MODIS. Terra+ Aqua land cover type yearly L3 global, 500.
- Gong, C., Xian, C., Cui, B., He, G., Wei, M., Zhang, Z., Ouyang, Z., 2021. Estimating NO<sub>x</sub> removal capacity of urban trees using stable isotope method: a case study of Beijing, China. *Environ. Pollut.* 290, 118004.
- Gong, C., Xian, C., Ouyang, Z., 2022. Assessment of NO<sub>2</sub> purification by urban forests based on the i-tree eco model: case study in Beijing, China. *Forests.* 13, 369.
- Guidolotti, G., Salvato, M., Calfapietra, C., 2016. Comparing estimates of EMEP MSC-W and UFORE models in air pollutant reduction by urban trees. *Environ. Sci. Pollut. Res.* 23, 19541–19550.
- Hirabayashi, S., 2011. Urban Forest Effects-Dry Deposition (UFORE-D) Model Enhancements. Citeseer.
- Hu, H., 1935. Distribution of population in China-additional statistical table and density chart. *Acta Geograph. Sin.* 2, 33–74.
- Hu, W., Si, B., 2021. Improved partial wavelet coherency for understanding scale-specific and localized bivariate relationships in geosciences. *Hydrol. Earth Syst. Sci.* 25 (1), 321–331.
- Huang, S., Li, X., Wu, B., Pei, L., 2010. Analysis of land degradation and driving forces in Three North Shelterbelt Project Area in recent 25 years. *Acta Geograph. Sin.* 67, 589–598.
- Hussain, M., Mahmud, I., 2019. pyMannKendall: a python package for non parametric Mann Kendall family of trend tests. *J. Open Source Softw.* 4, 1556.
- Li, X., Feng, L., Huang, C., Yan, X., Zhang, X., 2014. Chemical characteristics of atmospheric fallout in the south of Xi'an during the dust episodes of 2001–2012 (NW China). *Atmos. Environ.* 83, 109–118.
- Lin, J., Kroll, C.N., Nowak, D.J., 2021. An uncertainty framework for i-tree eco: a comparative study of 15 cities across the United States. *Urban For. Urban Green.* 60, 127062.
- Lovett, G.M., 1994. Atmospheric deposition of nutrients and pollutants in North America: an ecological perspective. *Ecol. Appl.* 4, 629–650.
- Malakar, P., Mukherjee, A., Bhanja, S.N., Ganguly, A.R., Ray, R.K., Zahid, A., Sarkar, S., Saha, D., Chattopadhyay, S., 2021. Three decades of depth-dependent groundwater response to climate variability and human regime in the transboundary Indus-Ganges-Brahmaputra-Meghna mega river basin aquifers. *Adv. Water Resour.* 149, 103856.
- Muñoz Sabater, J., 2019. ERA5-land monthly averaged data from 1981 to present, Copernicus climate change service (C3S) climate data store (CDS). *Earth Syst. Sci. Data*, 55, 5679–5695.
- Myneni, R., Park, T., 2021. MODIS/Terra+ Aqua Leaf Area Index/FPAR 4-Day L4 Global 500 M SIN Grid V061. The Land Processes Distributed Active Archive Center (LP DAAC): Sioux Falls, SD, USA.
- Nowak, D.J., 2021. Understanding I-Tree: 2021 Summary of Programs and Methods. General Technical Report NRS-200-2021.. US Department of Agriculture, Forest Service, Northern Research Station, Madison, WI, 100 p., 200, 1–100.
- Nowak, D.J., Crane, D.E., 2000. The Urban Forest Effects (UFORE) Model: Quantifying urban forest structure and functions. In: Hansen, Mark, Burk, Tom (Eds.), Integrated tools for natural resources inventories in the 21st century. Gen. Tech. Rep. NC-212. US Dept. of Agriculture, Forest Service, North Central Forest Experiment Station, St. Paul, MN, pp. 714–720, 212.
- Nowak, D.J., Crane, D.E., Stevens, J.C., 2006. Air pollution removal by urban trees and shrubs in the United States. *Urban For. Urban Green.* 4, 115–123.
- Nowak, D.J., Crane, D.E., Stevens, J.C., Hoehn, R.E., Walton, J.T., Bond, J., 2008. A ground-based method of assessing urban forest structure and ecosystem services. *Abric. Urban For.* 34 (6), 347–358.
- Nowak, D.J., Hirabayashi, S., Bodine, A., Greenfield, E., 2014a. Tree and forest effects on air quality and human health in the United States. *Environ. Pollut.* 193, 119–129.
- Nowak, D.J., Hirabayashi, S., Bodine, A., Hoehn, R., 2014b. Author's response to letter by Whitlow et al. *Environ. Pollut.* 257.
- Nowak, D.J., Hirabayashi, S., Doyle, M., McGovern, M., Pasher, J., 2018. Air pollution removal by urban forests in Canada and its effect on air quality and human health. *Urban For. Urban Green.* 29, 40–48.
- Pace, R., Guidolotti, G., Baldacchini, C., Pallozzi, E., Grote, R.D., Nowak, D.J., Calfapietra, C., 2021. Comparing i-tree eco estimates of particulate matter deposition with leaf and canopy measurements in an urban Mediterranean holm oak forest. *Environ. Sci. Technol.* 55, 6613–6622.
- Pretsch, H., Biber, P., Uhli, E., Dahlhausen, J., Rötzer, T., Caldentey, J., Pauleit, S., 2015. Crown size and growing space requirement of common tree species in urban centres, parks, and forests. *Urban For. Urban Green.* 14 (3), 466–479.
- Pullman, M., 2008. Conifer PM2.5 deposition and resuspension in wind and rain events.
- Qin, H., Jin, X., Guo, K., 2020. An overview of China's vegetation and plant diversity. Conservation and Reintroduction of Rare and Endangered Plants in China, pp. 3–19.
- Rahman, M.M., McConnell, R., Schlaerth, H., Ko, J., Silva, S., Lurmann, F.W., Palinkas, L., Johnston, J., Hurlburt, M., Yin, H., 2022. The effects of coexposure to extremes of heat and particulate air pollution on mortality in California: implications for climate change. *Am. J. Respir. Crit. Care Med.* 206, 1117–1127.
- Sæbø, A., Popek, R., Nawrot, B., Hanslin, H.M., Gawronski, H., Gawronski, S.W., 2012. Plant species differences in particulate matter accumulation on leaf surfaces. *Sci. Total Environ.* 427, 347–354.
- Schwartz, J., Dockery, D.W., Neas, L.M., 1996. Is daily mortality associated specifically with fine particles? *J. Air Waste Manage. Assoc.* 46, 927–939.
- Shah, A.M., Liu, G., Huo, Z., Yang, Q., Zhang, W., Meng, F., Yao, L., Ulgiati, S., 2022. Assessing environmental services and disservices of urban street trees. An application of the energy accounting. *Resour. Conserv. Recycl.* 186, 106563.
- Slinn, W.G.N., 1982. Predictions for particle deposition to vegetative canopies. *Atmos. Environ.* 16 (7), 1785–1794.

- Tai, A.P., Mickley, L.J., Jacob, D.J., 2010. Correlations between fine particulate matter ( $PM_{2.5}$ ) and meteorological variables in the United States: implications for the sensitivity of  $PM_{2.5}$  to climate change. *Atmos. Environ.* 44, 3976–3984.
- Tiwary, A., Sinnett, D., Peachey, C., Chalabi, Z., Vardoulakis, S., Fletcher, T., Leonardi, G., Grundy, C., Azapagic, A., Hutchings, T.R., 2009. An integrated tool to assess the role of new planting in  $PM_{10}$  capture and the human health benefits: a case study in London. *Environ. Pollut.* 157, 2645–2653.
- Velásquez Ciro, D., Cañón Barriga, J.E., Hoyos Rincón, I.C., 2021. The removal of  $PM_{2.5}$  by trees in tropical Andean metropolitan areas: an assessment of environmental change scenarios. *Environ. Monit. Assess.* 193, 1–16.
- Viana, M., Kuhlbusch, T.A., Querol, X., Alastuey, A., Harrison, R.M., Hopke, P.K., Hitzenberger, R., 2008. Source apportionment of particulate matter in Europe: a review of methods and results. *J. Aerosol Sci.* 39 (10), 827–849.
- Vos, P.E.J., Maiheu, B., Vankerkom, J., Janssen, S., 2013. Improving local air quality in cities: to tree or not to tree? *Environ. Pollut.* 183, 113–122.
- Wang, J., Xu, C., 2017. Geodetectors: principles and prospects. *Acta Geograph. Sin.* 72, 116–134.
- Wang, W., Chai, H., Ren, Z., Wang, X., Wang, S., Li, H., Gao, R., Xue, L., Peng, L., Zhang, X., Zhang, Q., 2019. Process, achievements and experience of air pollution control in China since the founding of the People's Republic of China 70 years ago. *Res. Environ. Sci.* 32, 1621–1635.
- Wang, B., Eum, K.-D., Kazemiparkouhi, F., Li, C., Manjourides, J., Pavlu, V., Suh, H., 2020. The impact of long-term  $PM_{2.5}$  exposure on specific causes of death: exposure-response curves and effect modification among 53 million US Medicare beneficiaries. *Environ. Health* 19, 1–12.
- Wei, J., Li, Z., Guo, J., Sun, L., Huang, W., Xue, W., Fan, T., Cribb, M., 2019. Satellite-derived 1-km-resolution  $PM_1$  concentrations from 2014 to 2018 across China. *Environ. Sci. Technol.* 53 (22), 13265–13274. <https://doi.org/10.1021/acs.est.9b03258>.
- Wei, J., Li, Z., Xue, W., Sun, L., Fan, T., Liu, L., Su, T., Cribb, M., 2021a. The ChinaHigh  $PM_{10}$  dataset: generation, validation, and spatiotemporal variations from 2015 to 2019 across China. *Environ. Int.* 146, 106290 <https://doi.org/10.1016/j.envint.2020.106290>.
- Wei, J., Li, Z., Lyapustin, A., Sun, L., Peng, Y., Xue, W., Su, T., Cribb, M., 2021b. Reconstructing 1-km-resolution high-quality  $PM_{2.5}$  data records from 2000 to 2018 in China: spatiotemporal variations and policy implications. *Remote Sens. Environ.* 252, 112136.
- Wei, J., Li, Z., Li, K., Dickerson, R., Pinker, R., Wang, J., Liu, X., Sun, L., Xue, W., Cribb, M., 2022. Full-coverage mapping and spatiotemporal variations of ground-level ozone ( $O_3$ ) pollution from 2013 to 2020 across China. *Remote Sens. Environ.* 270, 112775 <https://doi.org/10.1016/j.rse.2021.112775>.
- Wei, J., Li, Z., Wang, J., Li, C., Gupta, P., Cribb, M., 2023. Ground-level gaseous pollutants ( $NO_2$ ,  $SO_2$ , and  $CO$ ) in China: daily seamless mapping and spatiotemporal variations. *Atmos. Chem. Phys.* 23, 1511–1532. <https://doi.org/10.5194/acp-23-1511-2023>.
- Whitlow, T.H., Pataki, D.A., Alberti, M., Pincetl, S., Setala, H., Cadenasso, M., Felson, A., McComas, K., 2014. Response to authors' reply regarding "Modeled  $PM_{2.5}$  removal by trees in ten US cities and associated health effects" by Nowak et al. (2013). *Environ. Pollut.* 258, 259.
- Wu, H., Yu, X., Shi, Z., Zhang, Y., Zhang, Z., 2012. Advances in the study of  $PM_{2.5}$  characteristic and the regulation of forests to  $PM_{2.5}$ . *Sci. Soil Water Conserv.* 10, 116–122.
- Wu, S., Zhao, W., Yao, J., Jin, J., Zhang, M., Jiang, G., 2022. Precipitation variations in the Tai Lake Basin from 1971 to 2018 based on innovative trend analysis. *Ecol. Indic.* 139, 108868.
- Xie, L., Huang, F., Gan, X., Wen, X., Huang, Y., 2017. Research progress on the purification effects of urban forest vegetation on atmospheric particulate pollution matter. *For. Environ. Sci.* 33, 96–103.
- Yang, J., McBride, J., Zhou, J., Sun, Z., 2005. The urban forest in Beijing and its role in air pollution reduction. *Urban For. Urban Green.* 3, 65–78.
- Yang, J., Chang, Y., Yan, P., 2015. Ranking the suitability of common urban tree species for controlling  $PM_{2.5}$  pollution. *Atmos. Pollut. Ees.* 6 (2), 267–277.
- Yin, Z., Zhang, Y., Ma, K., 2022. Evaluation of  $PM_{2.5}$  retention capacity and structural optimization of urban park green spaces in Beijing. *Forests.* 13, 415.
- Zhai, H., Yao, J., Wang, G., Tang, X., 2022a. Impact of land use on atmospheric particulate matter concentrations: a case study of the Beijing–Tianjin–Hebei region, China. *Atmosphere.* 13, 391.
- Zhai, H., Yao, J., Wang, G., Tang, X., 2022b. Spatio-temporal characteristics and variation pattern of the atmospheric particulate matter concentration: a case study of the Beijing–Tianjin–Hebei region, China. *Atmosphere.* 13, 120.
- Zhai, H., Yao, J., Wang, G., Tang, X., 2022c. Study of the effect of vegetation on reducing atmospheric pollution particles. *Remote Sens.* 14, 1255.
- Zhao, C., Wang, Y., Wang, Y.Q., Zhang, H., 2013. Interactions between fine particulate matter ( $PM_{2.5}$ ) and vegetation: a review. *Chin. J. Ecol.* 32, 2203–2210.
- Zinke, P.J., 1967. Forest interception studies in the United States. *Forest Hydrol.* 8, 137–161.